Anatomy of North Pacific Decadal Variability

NIKLAS SCHNEIDER, ARTHUR J. MILLER, AND DAVID W. PIERCE

Scripps Institution of Oceanography, La Jolla, California

(Manuscript received 4 December 2000, in final form 9 July 2001)

ABSTRACT

A systematic analysis of North Pacific decadal variability in a full-physics coupled ocean–atmosphere model is executed. The model is an updated and improved version of the coupled model studied by Latif and Barnett. Evidence is sought for determining the details of the mechanism responsible for the enhanced variance of some variables at 20–30-yr timescales. The possible mechanisms include a midlatitude gyre ocean–atmosphere feedback loop, stochastic forcing, remote forcing, or sampling error.

Decadal variability in the model is expressed most prominently in anomalies of upper-ocean streamfunction, sea surface temperature (SST), and latent surface heat flux in the Kuroshio–Oyashio extension (KOE) region off Japan. The decadal signal off Japan is initiated by changes in strength and position of the Aleutian low. The atmospheric perturbations excite SST anomalies in the central and eastern North Pacific (with opposing signs and canonical structure). The atmospheric perturbations also change the Ekman pumping over the North Pacific, which excites equivalent barotropic Rossby waves that carry thermocline depth perturbations toward the west. This gyre adjustment results in a shift in the border between subtropical and subpolar gyres after about five years. This process consequently excites SST anomalies (bearing the same sign as the central North Pacific) in the KOE region. The SST anomalies are generated by subsurface temperature anomalies that are brought to the surface during winter by deep mixing and are damped by air–sea winter heat exchange (primarily latent heat flux). This forcing of the atmosphere by the ocean in the KOE region is associated with changes of winter precipitation over the northwestern Pacific Ocean. The polarity of SST and Ekman pumping is such that warm central and cool eastern Pacific anomalies are associated with a deep thermocline, a poleward shift of the border between subtropical and subpolar gyres, and warm SST anomalies and an increase of rain in the KOE region.

The preponderance of variance at decadal timescales in the KOE results from the integration of stochastic Ekman pumping along Rossby wave trajectories. The Ekman pumping is primarily due to atmospheric variability that expresses itself worldwide including in the tropical Pacific. A positive feedback between the coupled model KOE SST (driven by the ocean streamfunction) and North Pacific Ekman pumping is consistent with the enhanced variance of the coupled model at 20–30-yr periods. However, the time series are too short to unambiguously distinguish this positive feedback hypothesis from sampling variability. No evidence is found for a midlatitude gyre ocean–atmosphere delayed negative feedback loop.

Comparisons with available observations confirm the seasonality of the forcing, the up to 5-yr time lag between like-signed central North Pacific and KOE SST anomalies, and the associated damping of SST in the KOE region by the latent heat flux. The coupled model results also suggest that observed SST anomalies in the KOE region may be predictable from the history of the wind-stress curl over the North Pacific.

1. Introduction

Climate variations at decadal timescales profoundly influence human activities. The possibility of their prediction requires investigating the underlying physics. This can be viewed as consisting of two parts. First, the relationship of different variables and their physical linkage has to be established. Second, the processes determining the decadal timescale of the climate anomalies need to be understood. Analogous to a simple oscillator, the first task is concerned with the multivariate polarization relation or ''anatomy'' of decadal variability, while the second is concerned with its dynamics. Here, the polarization relation and processes underlying the timescale of decadal variability in the North Pacific are analyzed in a simulation with a coupled ocean–atmosphere model and available observations.

With observations of a major climate shift in 1976/77, the North Pacific is an area of particular interest for studies of decadal variability. This climate shift consisted of a cooling in the central North Pacific surrounded to the east, north, and south by warm anomalies (Nitta and Yamada 1989). This shift in sea surface temperature (SST) was caused by changes of surface heat flux, mixing, and Ekman advection (Miller et al. 1994) associated with a deeper and eastward shifted Aleutian low pressure system (Trenberth and Hurrel 1994) and increases in wintertime midlatitude westerlies (Hanawa et al.

Corresponding author address: N. Schneider, Scripps Institution of Oceanography, Mail Code 0224, 9500 Gilman Dr., La Jolla, CA 92093-0224.
E-mail: nschneider@ucsd.edu

1996). The subsurface oceanic response included changes of the midlatitude oceanic transport (Miller et al. 1998; Deser et al. 1999) that lagged those of the winds by about five years, and a shift to subduction of colder water from the surface central Pacific into the thermocline (Deser et al. 1996). The associated anomalies of thermocline depth (Schneider et al. 1999a) and ocean heat content (Tourre et al. 1999) propagated from the central Pacific in a southwestward direction to the subtropical Pacific. The delayed change of the midlatitude gyre caused temperature anomalies in the Kuroshio–Oyashio extension (KOE) region (Miller and Schneider 2000) that could not be explained by contemporaneous local atmospheric forcing (Xie et al. 2000) and were independent of contemporaneous SST variation in the central Pacific (Nakamura et al. 1997).

These North Pacific changes affected the ecosystem (Ebbesmeyer et al. 1991) and salmon catch (Mantua et al. 1997), and were associated with climate anomalies over North America (Latif and Barnett 1994), a modulation of the North American teleconnected response due to ENSO (Gershunov and Barnett 1998), and possibly a decadal modulation of the tropical variability (Barnett et al. 1999a; Pierce et al. 2000). Clearly, prediction of decadal variability in the North Pacific is highly desirable.

Studies into the causes of midlatitude decadal variability often focus on whether decadal variability in the midlatitudes involves a coupled ocean–atmosphere mode rather than merely reflecting forcing of the ocean by stochastic variability of the atmosphere. For example, Latif and Barnett (1994, 1996) proposed that an anomalously strong subtropical gyre generates SST anomalies in the North Pacific that then grow via a positive feedback between SST and the overlying atmosphere. The resulting atmospheric response in wind stress curl spins down the subtropical gyre after a lag of many years that reverses the sign of the North Pacific SST anomaly and initiates the opposite phase of a 20-yr oscillation. Robertson (1996) concluded similarly that a 300-yr integration of a low-resolution coupled model indicated that enhanced variance at a period of 18 years resulted from coupled interactions. However, a longer model integration did not reveal any special interactions at this timescale so that coupling accounted for only a tiny fraction of the decadal variance (Frankignoul et al. 2000).

From coupled model integrations with and without ocean dynamics Barnett et al. (1999b) and Pierce et al. (2001) concluded that decadal variability of SST in the central North Pacific results from internal atmospheric variability and heat storage in the mixed layer, while in the KOE the decadal variance is enhanced by ocean dynamics. Venzke et al. (2000) demonstrated that oceanic sea level changes in the western North Pacific result from North Pacific wind stress variations and are predictable several years into the future. Similarily Pierce et al. (2001) suggested that decadal variability of KOE SST is forced by remote wind stress curl anomalies over the North Pacific and spreads eastward to the date line by the currents. Pierce et al. (2001) identified a weak 20-yr spectral peak in KOE SST, heat content, upper-ocean meridional streamfunction, zonal advection, and latent heat flux that could not be explained by stochastically forced spatial resonance (Saravanan and McWilliams 1998; Neelin and Weng 1999). It was therefore attributed to a coupled feedback loop. To document the atmospheric feedback, Pierce et al. (2001) forced an atmospheric model with a typical SST anomaly pattern of the entire North Pacific. This revealed a significant atmospheric response in wind-stress curl that they suggested would drive ocean circulation that reverses the initial SST anomaly.

While elements of a decadal, midlatitude coupled mode are present, the fundamental physical mechanism and coupled nature of North Pacific decadal variability remains uncertain. For example, the rejection of the stochastically forced spatial resonance hypothesis by Pierce et al. (2001) involved analysis of KOE SST anomalies forced by basinwide stochastic wind-stress curl and stochastic heat fluxes, but in the KOE region SST anomalies are actually damped by the air–sea heat fluxes, not forced. The atmospheric response experiments involve anomalies of SST over the entire North Pacific including the central North Pacific where SST anomalies are forced directly by the atmosphere (e.g., Latif and Barnett 1994). It is unknown if KOE SST anomalies alone would have caused such a response.

This study is a systematic analysis of North Pacific decadal variability in a coupled model. The model is an updated and improved version of the model from which Latif and Barnett (1994, 1996) identified a 20-yr coupled air–sea mode. Following their hypothesis, relationships will be determined among ocean circulation anomalies that carry the decadal ''memory'' and fields such as atmospheric pressure, SST, and oceanic heat budgets in the central Pacific and KOE region. Of special interest are linkages between stochastic forcing and the delayed oceanic and regional atmospheric responses, and the consistency of the decadal variability with coupled ocean–atmosphere dynamics and with observations.

The results of this study may be important in constraining the fundamental assumptions invoked in simple models of North Pacific decadal variability (e.g., Jin 1997; Goodman and Marshall 1999; Talley 1999; Neelin and Weng 1999; Münnich et al. 1998; Cessi 2000; Watanabe and Kimoto 2000a). The effects of Rossby wave propagation in establishing a delayed negative feedback response by the ocean, the link between geostrophic circulation anomalies and SST, and the structure of atmospheric response to North Pacific SST anomalies are three crucial processes that are often posited in these simple models.

In the following, we review the coupled model (section 2), and show the decadal index time series of the oceanic streamfunction (section 3). To extract the large-

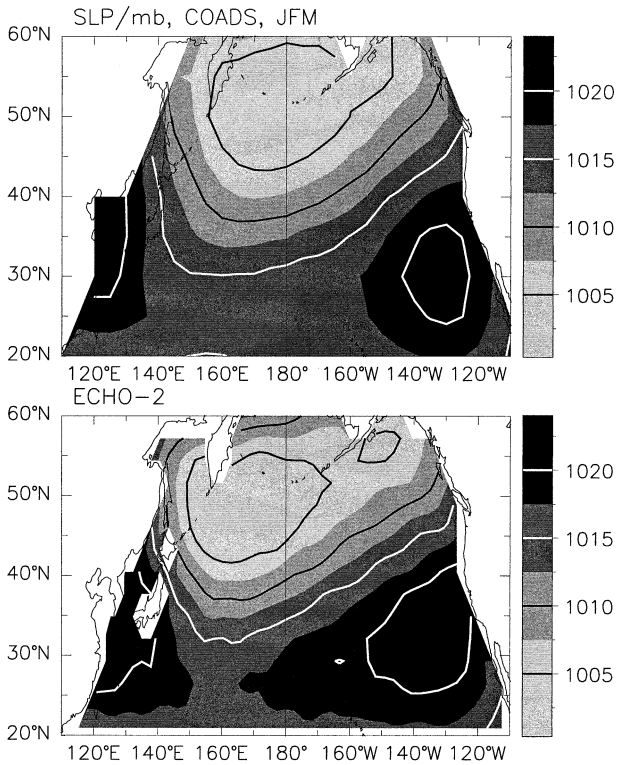

FIG. 1. Winter (Jan/Mar) SLP (mb) from COADS observations (top, Cayan 1992) and as simulated by ECHO-2 (bottom).

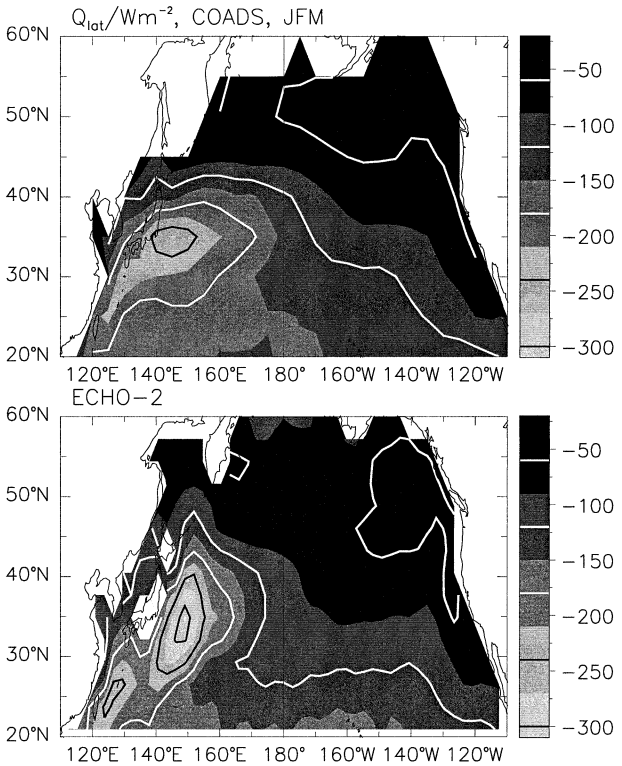

FIG. 2. Average latent heat flux (W m^{-2}) for Jan/Mar (JFM) from COADS observations (top, Cayan 1992) and as simulated by ECHO-2 (bottom).

scale context of this signal we employ complex empirical orthogonal functions (section 4). The time evolution (section 5) and multivariate polarization relation of decadal variability are presented (section 6). We then revisit the question of coupled air–sea mode and timescale selection (section 7). Finally results of the coupled model are compared with observations (section 8) and conclusions are presented (section 9).

2. The coupled model

The coupled model is an improved version of the model studied by Latif and Barnett (1994, 1996). The model, called ECHO-2, is described in detail by Frey et al. (1997). Its oceanic component is a primitive equation general circulation model with 20 levels in the vertical and a horizontal resolution of 2.8° latitude and longitude in the midlatitudes. Toward the Tropics the resolution increases to 0.5° latitude to better represent the equatorial waveguide. The atmospheric component is a 19-level, spectral model at a T-42 trapezoidal resolution (Roeckner et al. 1996). It employs a suite of subgrid-scale parameterizations. Within 60° latitude of the equator, the ocean and atmosphere exchange momentum, heat, and freshwater without flux correction. Poleward of 60° latitude, SST and salinity are relaxed to observed climatologies. The last 128 years of a 147-yr integration of the coupled ocean–atmosphere model are investigated here.

Overall, the mean state, seasonal cycle, and interannual variability of the simulations are realistic (Frey et al. 1997; Pierce et al. 2000). In the North Pacific, simulated wintertime sea level pressure (Fig. 1) compares favorably to observations from the Comprehensive Ocean–Atmosphere Data Set (COADS; Cayan 1992) with minor differences in the location of the Aleutian low: in the model it is shifted slightly to the southwest compared to observations. Winter latent heat fluxes (Fig. 2) are largest off Japan in the model and in observations (Cayan 1992), with values in ECHO-2 as large as 300 W m^{-2}, slightly larger than in observations. On the other hand, along 35°N high values extend farther to the east in observations than in the model. SSTs also compare well with observations from COADS (not shown), although the strong meridional gradient in the western North Pacific between 35° and 45°N is limited to the region near Japan instead of extending to the date line. Dynamic height, as represented by sea level, was estimated from pressure relative to a level of no motion at 1000 m for both the model and observations (Levitus 1982). Compared to observations, the model produces a stronger sea level gradient off Japan (Fig. 3), which might be the result of the smoothing employed by Levitus. In the KOE along 35°–40°N, meridional gradients

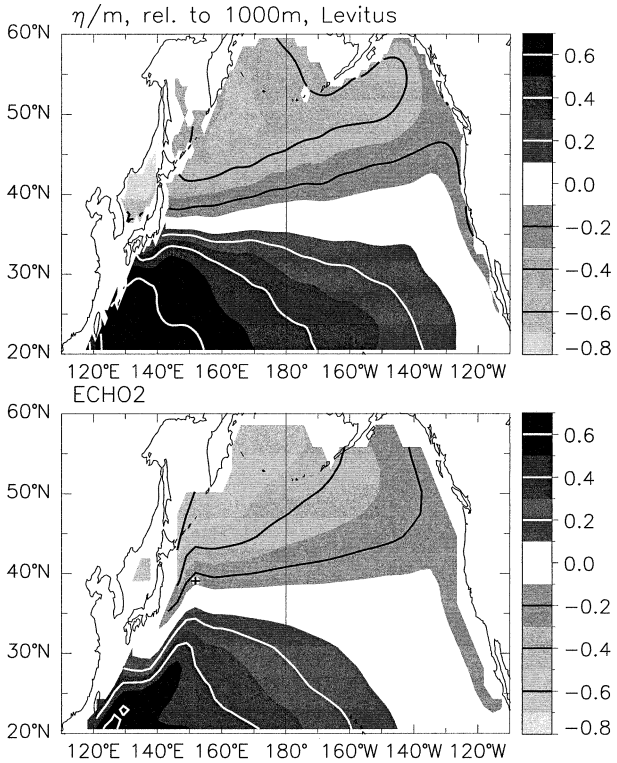

FIG. 3. Average sea level (m) relative to 1000 m estimated from (top) observations compiled by Levitus (1982) and from (bottom) temperature and salinity of ECHO-2. The "+" off Japan marks the position of the time series shown in Fig. 4.

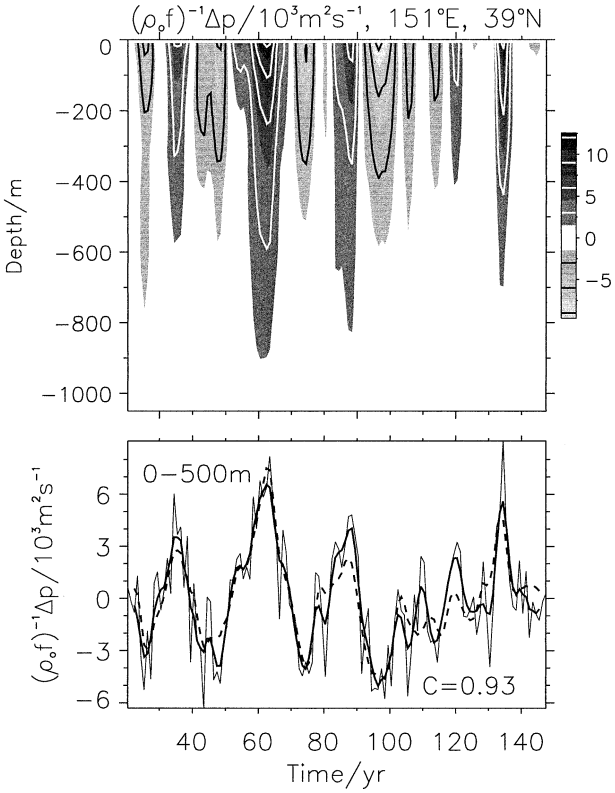

FIG. 4. (top) Oceanic streamfunction at 39°N, 151°E (see Fig. 3) as a function of time (yr) and depth (m). Units are 10^3 m^2 s^{-1} and contour and scale is presented by the grayscale on the right. Annually averaged values of model results have been detrended and smoothed with a five-point filter with linearly varying weights. (bottom) Time series of streamfunction vertically averaged between the surface and a depth of 500 m both unsmoothed (thin line) and smoothed (thick solid line). Superimposed is the reconstruction of the streamfunction from the leading CEOF alone (dashed line); its correlation with the original, smoothed data is 0.93.

of sea level are weaker in the model than in observations, and suggest less vigorous flows in the simulation.

Aspects of low-frequency variability in this simulation have been the subject of a number of studies. The driving of the Tropics by midlatitude decadal variability via an atmospheric bridge was suggested by Barnett et al. (1999a) and Pierce et al. (2000). The role of an oceanic bridge in the thermocline have been investigated by Pierce et al. (2000) and Schneider et al. (1999b). In the Tropics, a 10-yr mode, associated with the advection of temperature–salinity anomalies along isopycnal surfaces, was discussed by Schneider (2000).

The following analysis was performed on anomalies from the climatological monthly means, either as annual, seasonal, or monthly averages. A small linear trend, present primarily in subsurface, oceanic variables was removed. For all analyses (except spectra), annual, seasonal or monthly anomalies are smoothed with a normalized 1–2–3–2–1 filter applied to values of successive years. This retains variance at timescales from approximately 4 to 60 years.

3. North Pacific streamfunction

Following the hypothesis that the memory of midlatitude decadal variability resides in anomalies of the oceanic circulation, we choose the geostrophic streamfunction Ψ as the principal variable for analysis. It is estimated from total pressure p via

$$\Psi(x, y, z, t) = (\rho_0 f)^{-1}[p(x, y, z, t) - p(x_E, y, z, t)], \quad (1)$$

where ρ_0 is a reference oceanic density; f is the Coriolis parameter; x, y, z, are the zonal, meridional, and vertical coordinates; t is time; and x_E is the longitude of the eastern coast. The value of Ψ denotes the zonal pressure difference and the meridional, geostrophic transport per unit depth in the section between longitude x and the coast at x_E. Note that it differs from pressure by its value at the eastern boundary.

In the midlatitude North Pacific, the variance of Ψ is largest in the KOE region off Japan, and shows a pronounced decadal variability (Fig. 4). From year 20 to 105 the streamfunction undergoes a regular oscillation with a period of 20–30 yr. Accordingly, its spectrum is enhanced at periods of 21 and 33 yr (Pierce et al. 2001) that coincide with the spectral break from red to white

(see section 7). The majority of the decadal variability of Ψ is trapped in the upper 500 m, reminiscent of equivalent barotropic flow (Miller et al. 1998). A decomposition into baroclinic and barotropic (vertical average) components reveals the latter is roughly 5%–10% of the amplitude of baroclinic signals at the surface and is highly correlated (0.95) to the surface baroclinic signal at a lead of 1 yr.

4. Analysis procedure

The large-scale context and temporal evolution of this decadal signal is extracted using complex empirical orthogonal functions (CEOFs; Barnett 1983) of $\Psi(\underline{x}, t)$, where $\underline{x}$ denotes the position (x, y, z). The streamfunction is expanded as

$$\Psi(\underline{x}, t) = \Re\left[\sum_k A_k(t)e^{-\iota\varphi_k(t)}\Phi_k(\underline{x})\right], \qquad (2)$$

where $A_k(t)$ and $\varphi_k(t)$ are magnitude and phase of the complex eigenfunction of the covariance matrix of $\tilde{\Psi} := \Psi + \iota H(\Psi)$, H being the Hilbert transform. The complex, spatial loading patterns $\Phi_k(\underline{x})$ (in the following referred to as ''associated patterns'') are obtained by projection of $\tilde{\Psi}$ onto the principal component $A_k(t)\exp[-\iota\varphi_k(t)]$. Associated patterns of other variables Y are obtained similarly by projection of $\tilde{Y}$ onto the principal component $A_k \exp[-\iota\varphi_k]$.

The arbitrary phase between the principal component and associated pattern is fixed by minimizing the magnitude of the spatial correlation of the real and imaginary part of Φ_k. For ease of visualization and discussion, maps of the associated pattern will be shown for a typical value of A_k and for phases $\varphi_k = j/4\pi$, $j = 1, 2, 3, 4$, representing one-half of a cyle of the variability.

We chose a representation in CEOFs since it concisely shows the decadal evolution in terms of standing and propagating components that capture both contemporaneous and lagged covariances of Ψ and the associated variability of other fields. The principal component of the CEOF represents the time evolution, and the associated patterns of oceanic and atmospheric variables form the multivariate polarization vector of decadal variability. All results also could have been obtained with other methods, such as lagged correlation analysis, extended EOFs or a lagged regression analysis with an index time series of Ψ.

5. Time evolution of decadal variability

In the Tropics, Ψ has large variance that, when included, dominates the leading CEOFs at the expense of capturing variance of Ψ in the midlatitude Pacific and KOE. The CEOFs were therefore estimated from latitudes north of 25°N. The leading COEF reconstructs the decadal signal in the KOE (Fig. 4) with a very high correlation (0.93). This suggests that the associated pattern of this CEOF captures the basinwide spatial and temporal evolution of the decadal North Pacific variability.

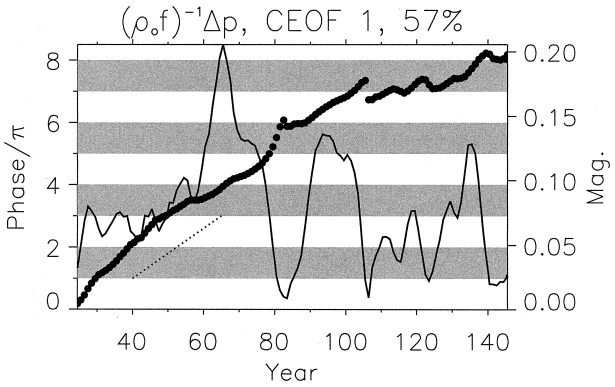

FIG. 5. Principal component (decadal index) of the leading CEOF of oceanic streamfunction as a function of time (yr). The complex principal component is represented by its phase in multiples of π (filled circles, ordinate on left, and alternating gray and white bands) and by its magnitude (solid line and ordinate on right). The slope of the phase corresponding to a period of 25 yr is denoted by a dotted line. The CEOF explains 57% of the detrended and smoothed streamfunction in the Pacific from 25° to 60°N and throughout the water column.

The amplitude of the leading principal component (Fig. 5) is approximately constant until year 50 and then undergoes two dramatic events, with peak amplitudes in years 63 and 91, and small values in years 81 and 104. In later years the magnitude is variable and largest around year 133. The phase, φ_1, of the leading CEOF increases consistently at an average rate of 25 years per cycle. Typically, local maxima of the magnitude occur when $\mathrm{mod}(\varphi_1 + 2n\pi, \pi) = \pi/2$, $n = 1, 2, 3, \ldots$; local minima at modulus equal to 0. Before year 80, the phase advances by two and one-half cycles while amplitudes remain significant; the events centered at years 91 and 133 each last less than half a cycle. We will use this principal component of the leading CEOF as an index for the decadal variability and refer to it, for brevity, as ''decadal index.'' Associated pattern will be used exclusively to refer to the projection of any variable onto the decadal index.

6. Decadal polarization relation

a. Oceanic streamfunction

The associated pattern of the oceanic streamfunction vertically averaged over the top 500 m of the water column is shown in Fig. 6. It is predominantly a standing pattern with small values at $\varphi_1 = \pi/4$ and large values at $\varphi_1 = 3/4\pi$. The center of action is located at the border of the subtropical and subpolar gyres, and represents a latitudinal shift of the separation rather than a spinup of these gyres (Fig. 3). The signal originates east of the date line for $\varphi_1 = \pi/4$ and spreads to the western boundary while being intensified (transition to

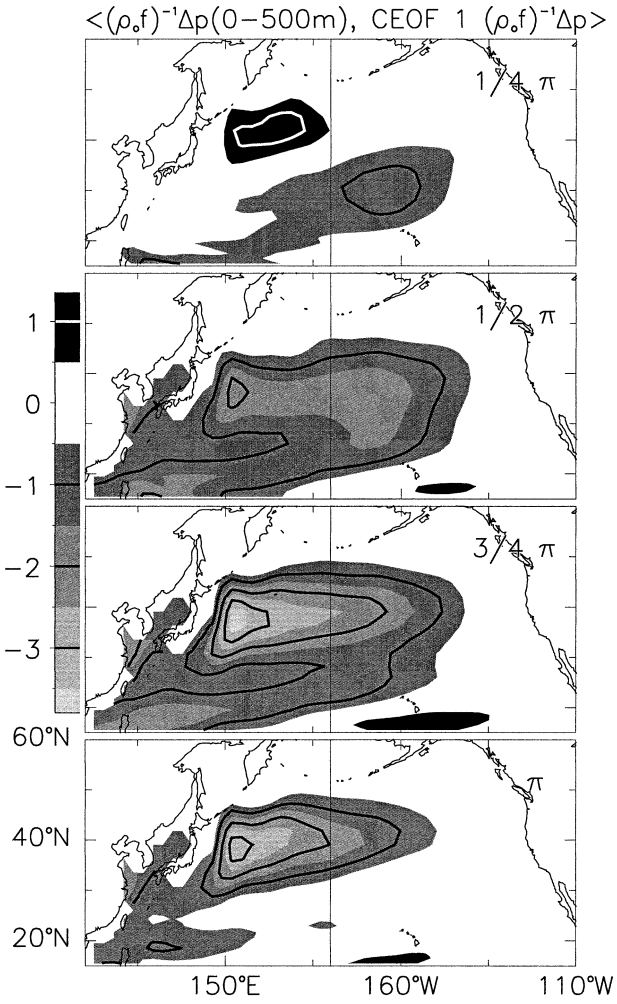

FIG. 6. Associated pattern of oceanic streamfunction, vertically integrated between the surface and a depth of 500 m, as a function of latitude and longitude. Results correspond to an amplitude of the CEOF of 0.1 and a modulus of the phase and 2π (from top panel down) of 1/4 π, 1/2 π, 3/4 π, and π (see Fig. 5). The next half of a cycle is obtained by reversing the sign of anomalies. Units are 10^3 $m^2\ s^{-1}$ and values are given by grayscale on left.

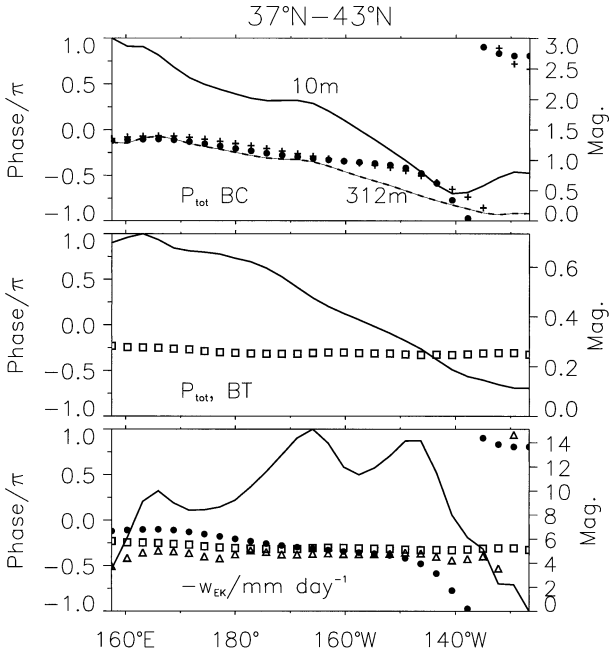

FIG. 7. Associated patterns of oceanic pressure ($m^2\ s^{-2}$, top and center) and Ekman pumping (mm day^{-1}, bottom) averaged from 35° to 45°N as a function of longitude. The complex patterns are represented by their phases (symbols, ordinates on left) and magnitudes (lines, ordinates on right). The top panel shows the baroclinic component of pressure at a depth of 10 m (solid line and filled circles) and at a depth of 312 m (dashed line and "+" symbols). The center panel displays the associated pattern of the barotropic component of pressure; note the magnified scale for the magnitude compared to the top panel. The bottom panel shows the associated pattern of Ekman pumping (solid line and triangles) with reversed sign such that its phase is identical to the phase of the local ocean pressure response (i.e., upwelling causes low ocean pressure). For comparison, the phases of the baroclinic component at 10 m (filled circles) and of the barotropic component (squares) are replotted.

$\varphi_1 = \pi/2$) and via a secondary, weak branch, in a southwesterly direction toward 20°N. Through the next quarter of the cycle the anomalous circulation spans the entire North Pacific between 25° and 50°N and then slowly decays from the east.

This pattern explains more than 50% of the low-frequency Ψ variance in the midlatitudes and as much as 90% poleward of 30°N and west of the date line. The secondary signal is marked by a southwestwardly decaying local maxima of the explained variance, with values around 20% at 20°N, 135°E. South of 20°N the projection captures less than 20% of the variance. Thus the oceanic signal resides in the midlatitude and appears independent of oceanic variability in the Tropics.

To show the small propagating component around 40°N, the vertical structure, and the effect of signals originating at the eastern boundary, the associated pattern of oceanic pressure is shown in the top two panels of Fig. 7 for averages over the latitudes of largest signal (37°–43°N).

The associated pattern of the baroclinic component of pressure (Fig. 7, top) is surface intensified and vertically coherent. The magnitudes are largest at the surface and the phases are nearly identical at 10 and 312 m. Magnitudes at both depths increase monotonically westward from 140°W while the phases increase by approximately $\pi/4$ from the central Pacific to 160°E. This phase difference signifies a westward propagation of the baroclinic signals. For a nominal period of the decadal index of 20–25 yr, the corresponding lag between the central Pacific and the KOE region is roughly 5–6 yr.

In contrast, the phases of the associated pattern of the barotropic component of pressure (Fig. 7, middle) are nearly constant across the basin in accordance with the fast adjustment time of this mode compared to the decadal timescale. Similar to the baroclinic component, the magnitude of the barotropic component increases

toward the west, but is 4–5 times smaller that the surface baroclinic component.

At the eastern boundary, the magnitude of the associated pattern of pressure is small and indicates that coupling with the equatorial region via the eastern boundary processes such as Kelvin waves is not a major forcing mechanism for the midlatitude variability. In addition, this indicates that associated patterns of pressure and streamfunction can be interchanged.

Ekman pumping at the surface is the major forcing of oceanic streamfunction and pressure as shown by its associated pattern (Fig. 7, bottom). The associated Ekman pumping has the largest magnitude east of the date line and varies nearly in phase throughout the Pacific indicating a standing forcing pattern. The Ekman pumping determines the phase of both barotropic and baroclinic pressure (and Ψ) east of the date line where the forcing is largest. Westward, both the increasing magnitude and constant phase of the barotropic component are qualitatively consistent with Sverdrup dynamics. However, a quantitative comparison (not shown) reveals a slight westward attenuation of the pressure compared to the Sverdrup solution suggestive of the effects of friction in the diffusive, low-resolution ocean model.

b. Atmospheric pressure

The associated patterns of atmospheric pressure and concomitant Ekman pumping forcing are dominated by winter conditions, with summer perturbations having little relationship with the decadal index. Winter atmospheric pressure perturbations (Fig. 8) are largest at 35°N, 150°W and extend across the North Pacific. Compared to the mean pressure in winter (Fig. 1), perturbation pressure is largest in the gradient region between the Aleutian low and the subtropical high and corresponds to a meridional displacement of the mean field. The signals are largest and positive at $\varphi_1 = \pi/2$ to $3/4\pi$ when the oceanic streamfunction has maximum growth rate (downward Ekman pumping corresponding to positive streamfunction). In contrast, large streamfunction anomalies develop at the western boundary (at $\varphi_1 = 3/4\pi$ to π) when eastern North Pacific atmospheric pressure decreases; this indicates that the large streamfunction anomalies there are not locally forced, but are the integrated effect of the preceding forcing over the North Pacific.

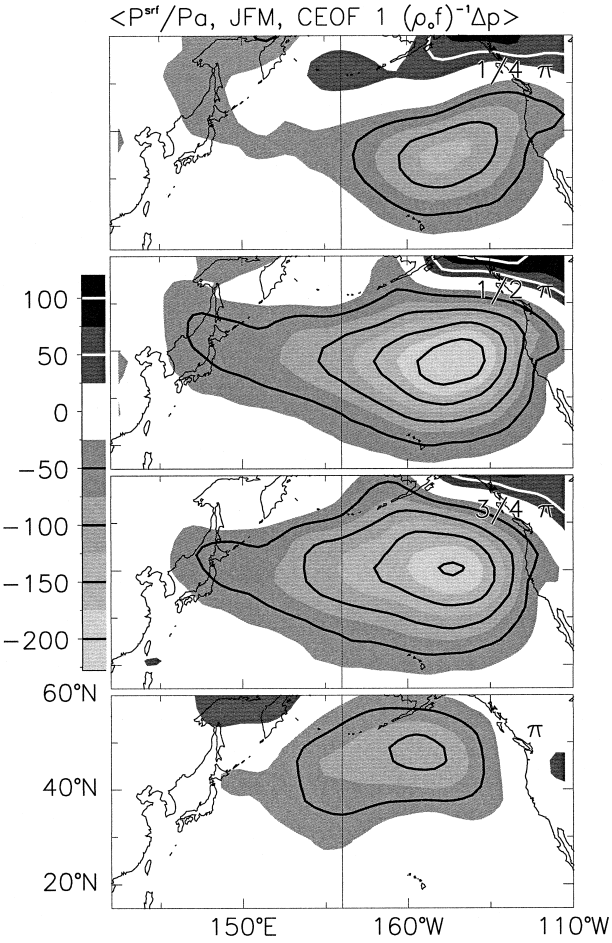

FIG. 8. Same as Fig. 6 but for winter (Jan–Mar) surface pressure (Pa).

c. SST and heat budget

1) CENTRAL NORTH PACIFIC

The associated pattern of the wintertime sea level pressure leaves a signature in SST that is largest during winter. The associated pattern of SST resembles the canonical, observed decadal pattern (e.g., Tanimoto et al. 1993) in the central North Pacific (Fig. 9). Anomalies centered at 35°N, 170°W are surrounded to the east, north, and south by anomalies of opposite sign, resembling a horseshoe.

To determine the physical forcing of these SST anomalies, the associated patterns of the surface-level (0–20-m depth) heat budget, air–sea heat flux, and SST are averaged over the central North Pacific. The terms of the heat budget are the rate of change of SST, the tendency due to horizontal temperature advection, the tendency due to vertical temperature advection and vertical ocean mixing, the effects the surface heat fluxes, and the remaining small terms such as horizontal mixing and numerical corrections. The surface heat flux consists of the shortwave, longwave radiative, and latent and sensible components. The sign convention of the heat budget components is such that positive values correspond to heating of the ocean.

In the central Pacific around 35°N, the associated patterns of SST and horizontal advection are in phase (Fig. 10), as shown by their alignment in the complex plane. Advection is dominated by Ekman advection as revealed by a comparison with the associated pattern of wind stress (not shown). This heating tendency is balanced

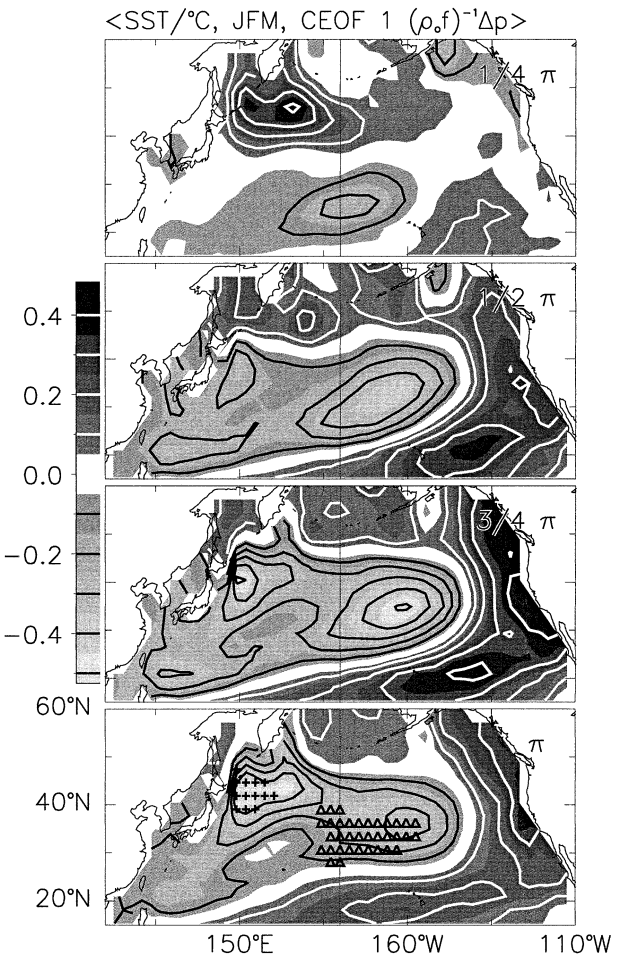

FIG. 9. Same as Fig. 6 but for winter (Jan–Mar) SST (K). Symbols denote areas in the KOE (plus) and in the central Pacific (CP, triangle) where detailed heat budgets are estimated.

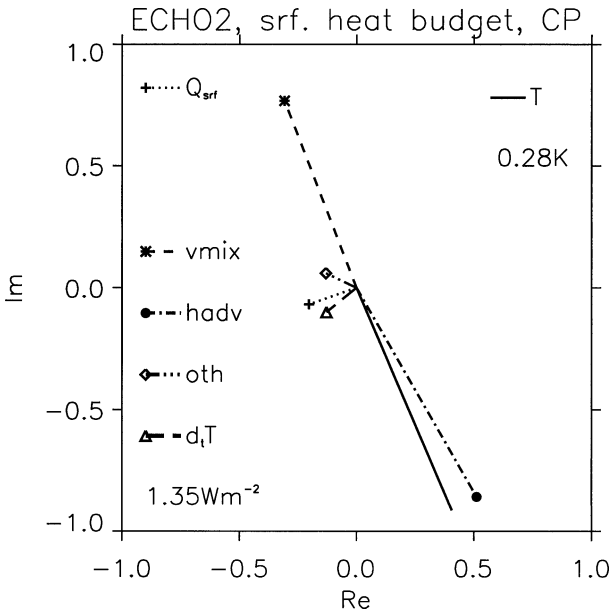

FIG. 10. Associated patterns of annually averaged anomalies of components of the heat budget of the topmost ocean level. Results have been averaged over the region CP in the central Pacific shown as triangles in Fig. 9 and are displayed in the complex plane. Temperature is displayed by the solid line and is normalized by 0.28 K. The heat flux components are shown by the broken lines and symbols and are normalized by 1.35 W m^{-2}. Heat flux components are the net air–sea heat exchange (Q_{srf}, dotted line and "+"), vertical mixing ("vmix" short dashes and "*"), horizontal advection ("hadv" dash–dot and solid circle), local rate of change ("d_tT," long dashes and triangle) and sum of remaining terms of the surface heat budget ("oth" dash–dot–dot and diamond). The angle between the lines corresponds to the lag between corresponding variables, and their lengths represent relative magnitudes. Thus, the heat budget shown is dominated by a balance of horizontal advection and vertical mixing, with horizontal advection forcing anomalies of SST. Other terms are of secondary importance.

by changes of winter time stratification and vertical mixing: during winter, warm surface anomalies are accompanied by subsurface anomalies of the same sign, but reduced magnitude, so that the vertical temperature gradient and the cooling tendency of vertical mixing increase. The associated pattern of heat storage and other terms are small; changes of the net air–sea heat exchange, in particular, are of secondary importance because anomalies of latent heat and shortwave heat fluxes, while both large and nearly aligned with SST, largely balance (Fig. 11). Thus, in the central Pacific, wind anomalies deform the SST field by changes of vertical mixing and Ekman advection. Associated changes of the latent heat flux are balanced by changes of cloudiness and incident shortwave radiation.

Northeast of Hawaii, where SST anomalies have opposite polarity (Fig. 9), the annual averaged surface heat budget is a small residual of a large annual cycle. SST anomalies are generated in winter months and partially removed during the subsequent summer (not shown) primarily by the latent heat flux suggestive of the "footprinting" mechanism (Vimont et al. 2001). During both seasons the tendency due to the air–sea fluxes is opposed by vertical mixing. Similary to the central Pacific pattern, SST anomalies are a therefore a direct response to atmospheric forcing.

The changes in wintertime SST shift the position of outcrops of isopycnals and thereby generate signals that subduct and move in the oceanic thermocline toward the south. The subducted anomaly can be seen as the secondary signal in the oceanic pressure (Fig. 6) that propagates from the central North Pacific in a southwesterly direction to 20°N. These anomalies can be traced for several years, but lose their coherent structure before reaching the equatorial upwelling region (Schneider et al. 1999b; Pierce et al. 2000).

2) KUROSHIO–OYASHIO EXTENSION

As the streamfunction anomalies in the western boundary region are established ($\varphi_1 = \pi/2$ to π), a secondary maximum of the associated SST pattern de-

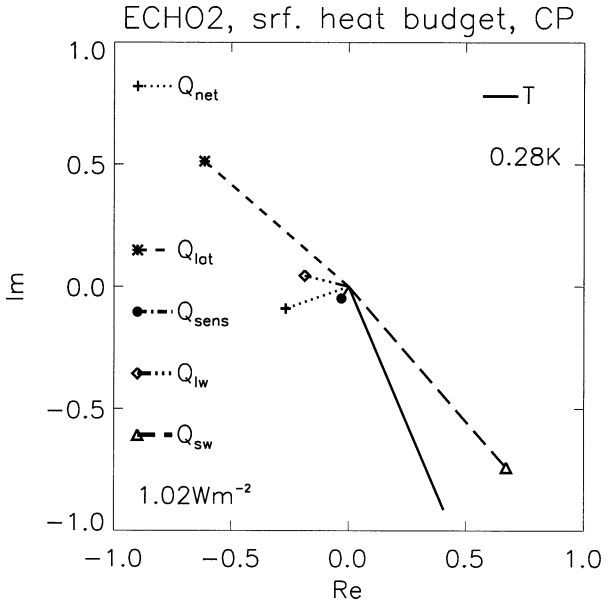

FIG. 11. Same as Fig. 10, but for annually averaged anomalies of SST (black line) and components of the air–sea exchange. Heat fluxes are scales by 1.02 W m^{-2}. The dotted line with "+" symbol represents the net heat flux, other lines represent the latent (Q_{lat}, short dashes and "*"), sensible (Q_{sens}, dash–dot and solid circle), longwave (Q_{lw}, dash–dot–dot and diamond) and shortwave (Q_{sw}, long dashes and triangle) heat fluxes. The sign of the air–sea heat fluxes is such that the projection of a component that damps anomalies of SST points in a direction opposite to the projection of SST.

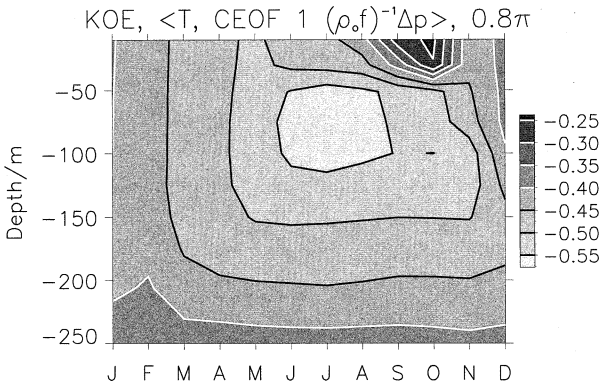

FIG. 12. Associated pattern of monthly values of temperature in the KOE region, as a function of calendar month and depth in m. The pattern is shown for a typical amplitude of leading CEOF and $\varphi_1 = 0.8\pi$. Contour levels are 0.05 K and scale is given on the right.

velops off Japan in the KOE region (Fig. 9). It is of the same sign as preceding anomalies in the central Pacific. To establish the seasonality of this signal, the associated pattern of oceanic temperature, averaged over the KOE region, is shown for every month of the year and as a function of depth. Since the phase of the associated pattern in this area is not a function of depth or time of year, it is displayed for $\varphi_1 = 0.8\pi$ corresponding to largest SST anomalies in the KOE region.

Below 50 m, the decadal temperature anomaly persists throughout the year (Fig. 12). In summer, the seasonal thermocline insulates the subsurface waters from surface forcing allowing large subsurface but unrelated surface temperature anomalies. In late fall and winter, increased mixing erodes the seasonal thermocline and brings the subsurface temperature perturbation to the surface, where it is vented to the atmosphere. The heat budget of the top layer (Fig. 13) consequently shows a quasi-steady balance of vertical mixing, via cold season entrainment that forces SST anomalies, and the air–sea heat transfer. In the surface layer, horizontal advection is an order of magnitude smaller. The location of SST anomalies at the northern half of the streamfunction anomalies suggests that anomalous obduction (Qui and Huang 1995) brings thermocline anomalies into the mixed layer by the displacement of ocean streamfunction relative to the wintertime meridional gradients of mixed layer depth.

The coupled model therefore indicates that anomalies of oceanic streamfunction cause subsurface temperature anomalies by vertical undulations of the thermocline, that affect KOE SST via vertical processes (mixing). Note that this mechanism for persistent SST anomalies in the KOE region differs from the SST reemergence mechanism (Namias and Born 1970, 1974; Alexander and Deser 1995; Alexander et al. 1999) where atmospheric wintertime forcing of SSTs leaves a subsurface imprint on a quiescent ocean that is reentrained into the mixed layer in the next cold season.

The net air–sea heat flux anomalies in the KOE damp the SST perturbations and are dominated by sensible and latent heat fluxes (Fig. 14). Their magnitude (roughly 10 W m^{-2}) dwarfs decadal anomalies of the air–sea heat flux elsewhere in the North Pacific. The oceanic origin of the thermal anomaly indicates that in the KOE region the ocean forces the atmosphere by anomalous fluxes of latent and sensible heat and moisture. This is in contrast to the central Pacific, where SST anomalies are generated by the contemporaneous atmosphere.

To summarize, in the KOE region the SST anomaly originates below the mixed layer by perturbations of the streamfunction. These temperature anomalies persist with KOE streamfunction anomalies while the central Pacific pattern withers. The KOE SST anomalies are damped by sensible and latent air–sea flux anomalies and thus force the midlatitude atmosphere.

d. Precipitation

The associated patterns of precipitation (Fig. 15) are strongest in winter and explain a significant portion of its low-frequency variability in the central Pacific and in the KOE region (correlation with total precipitation larger than 0.5). East of the date line, from 25° to 45°N and from 160° to 130°W the generation of the central Pacific streamfunction anomalies are associated with increased precipitation at the eastern flank of the wind stress pattern. The development of the warm (cool) SST

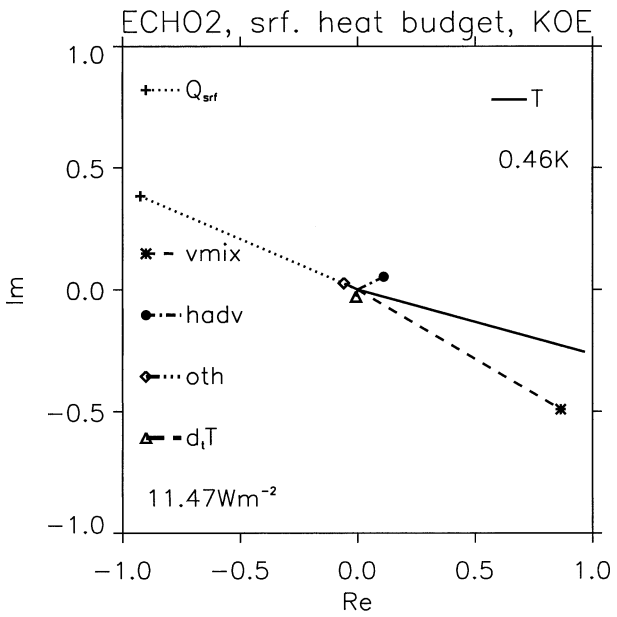

FIG. 13. Same as Fig. 10, but for KOE region (see Fig. 9).

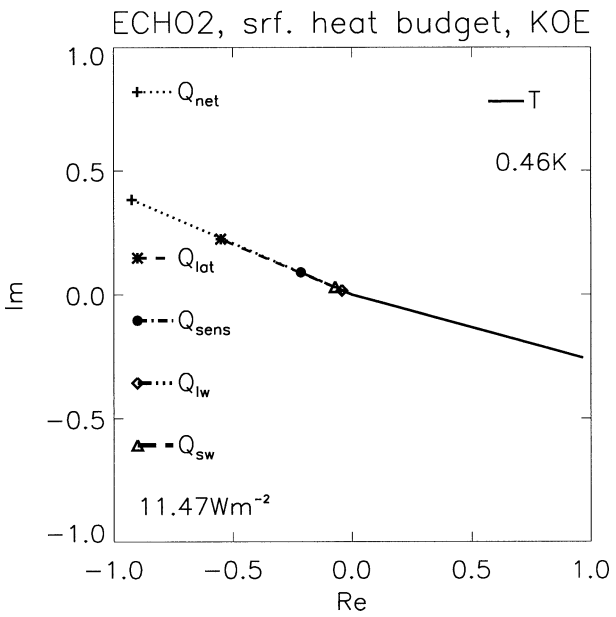

FIG. 14. Same as Fig. 11, but for the KOE region (see Fig. 9).

and associated venting of heat in the KOE region coincides with increased (decreased) precipitation to the east of Japan. Thus the oceanically induced perturbation in the KOE region leads to local precipitation and release of latent heat in the atmosphere and represents a midlatitude ocean-to-atmosphere coupling.

The details of this atmospheric response are not studied here. However, a heuristic explanation for this atmospheric response can be gleaned from the mean conditions in the KOE region. The time-averaged winter SST, turbulent air–sea heat fluxes (Fig. 2) and precipitation in the KOE region deviate strongly from mid-ocean conditions. This situation is caused by the land–sea contrast and the warm western boundary current. Thus we speculate, that the decadal anomalies of the western boundary currents modulate this time average condition and regulate the coupling between SST, air–sea fluxes, and precipitation via the same physics that is responsible for the mean conditions. In support of this argument, a recent study by Watanabe and Kimoto (2000b) found a response of midlatitude precipitation to SST anomalies in the western North Atlantic and explained these by midlatitude storm track changes.

e. Summary of decadal polarization relation

North Pacific decadal variability in this coupled model evolves like the schematic of Miller and Schneider (2000). Changes of the winter sea level pressure over the North Pacific are associated with an altered surface heat budget over the Pacific through changes in advection by Ekman currents, mixing, and air–sea heat exchange. The associated Ekman pumping forces anomalies of the oceanic streamfunction that affect, after several years, the KOE region. Deep mixed layers during winter bring these temperature anomalies in the thermocline to the surface and cause an SST anomaly. The SST signal is of the same sign as the preceding central Pacific SST anomaly. The oceanic perturbation of the winter, surface heat budget in the western boundary region is balanced primarily by changes of latent heat flux and affects precipitation there. This indicates at least a local response of the atmosphere to the oceanically induced air–sea heat flux perturbation.

7. Timescale selection

Decadal timescales dominate the variability of streamfunction in the KOE region (solid line in Fig. 16, left panel). In fact, variance at periods from 20 to 30 yr is enhanced compared to the adjacent spectral bands, yet this ''peak'' is not significant. At best, application of more sophisticated spectral techniques to determine its precise period (Pierce et al. 2001) indicate that this peak is barely significant.

The accumulation of stochastic atmospheric forcing along Rossby wave trajectories (Frankignoul et al. 1997) could account for the majority of the variance in the KOE region, the ''red'' spectrum of pressure, the irregular evolution of the decadal index (Fig. 5), and the enhanced variability at 20–30-yr periods (via stochastically forced ''spatial resonance'' or ''optimal forcing''; Saravanan and McWilliams 1998; Neelin and Weng 1999). Alternatively, the peak could result from a weak, midlatitude ocean–atmosphere feedback, from external forcing by, for example, variability in the Tropics (Trenberth 1990; Graham et al. 1994), or from sampling error.

In the following, we will test if Rossby wave dynam-

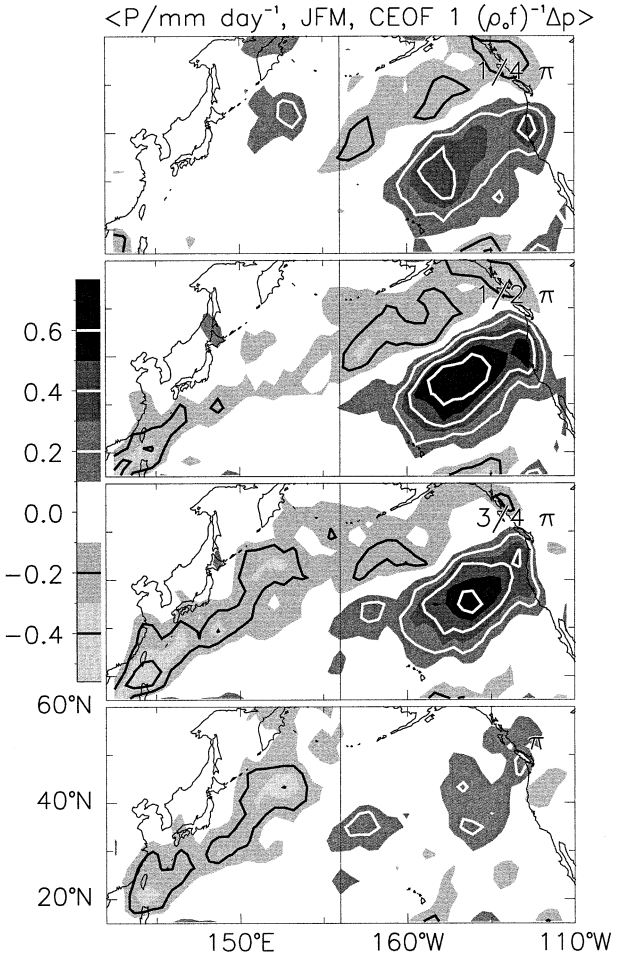

FIG. 15. Same as Fig. 6, but for winter (JFM) precipitation (mm day^{-1}).

ics fit the coupled model variability, and then use the resulting simple model to investigate if the enhanced variability at 20–30 yr is consistent with stochastic spatial resonance or a midlatitude, ocean–atmosphere feedback. The possible forcing from low-frequency variability outside of the North Pacific is then addressed by considering the global associated patterns of atmospheric variables.

a. Equivalent barotropic Rossby wave model

The associated patterns of oceanic pressure and Ekman pumping (Fig. 7) are qualitatively consistent with a forced Rossby wave (see section 6a). Thus, pressure P, vertically averaged between depth H and the surface, and normalized by the ocean's density ρ_0, should be governed by a linear vorticity balance of vortex stretching, meridional advection of planetary vorticity, forcing by the wind-stress curl, and dissipation

$$\partial_t P - c_0 \partial_x P = -\frac{P}{r_0} + \frac{f c_0}{\beta H \rho_0} F \qquad (3)$$

on a midlatitude β plane. Here, c_0 is the westward propagation speed of long, nondispersive Rossby waves, H is the depth of the active layer, f is the Coriolis parameter at the reference latitude, β its meridional derivative, and F is the vertical component of the curl of the wind stress. Horizontal mixing is parameterized as a Newtonian decay with a timescale r_0 and is needed since the barotropic pressure signal is underestimated by the Sverdrup balance westward of the forcing regions (not shown). It represents the effect of meridional horizontal mixing and scales as L_y^2/A_H, where L_y is a typical meridional length scale, and A_H is horizontal eddy viscosity. Explicit horizontal mixing in the zonal direction is not included due to the large zonal scales of midocean streamfunction anomalies. This process is only required for the calculation of the western boundary currents in a Munk layer but does not determine the western boundary transport (or the pressure at the eastern end of the western boundary current) that is of interest here. A similar Rossby wave model (without the Newtonian decay) was invoked by Sturges and Hong (1995) to explain low-frequency sea level fluctuation off Bermunda by North Atlantic wind-stress variability, and by Akimoto et al. (1996) to explore thermocline depth and Kuroshio transport variations in the subtropical Pacific.

The solution for pressure

$$P(x, t) = -\frac{f}{\beta H \rho_0} \int_{x_E}^{x} dx' \exp\left(-\frac{x' - x}{r_0 c_0}\right) F\left(x', t - \frac{x' - x}{c_0}\right) + \exp\left(-\frac{x_E - x}{r_0 c_0}\right) P\left(x_E, t - \frac{x_E - x}{c_0}\right) \qquad (4)$$

shows two effects: interior wind-stress curl forcing and eastern boundary pressure forcing. Rossby waves emanate from the eastern boundary at x_E with prescribed amplitudes, and accumulate wind-stress curl forcing along their trajectories. Dissipation modifies the solution by discriminating against wind stress and boundary conditions eastward of a distance of $r_0 c_0$.

The Rossby wave propagation speed c_0 and decay timescale r_0 are determined by fitting Eq. (4) to the results of ECHO-2. Specifically, the midlatitude oceanic decadal variation of ECHO-2 (Fig. 4) is represented by the model's pressure in the Pacific, averaged vertically from the surface to a depth of 500 m and meridionally from 34° to 41°N. The model's wind stress curl and eastern boundary condition are obtained by the same meridional average. Minimizing the difference of the results of Eq. (4) from ECHO-2's pressure in the KOE region and at several longitudes toward the central Pacific, yields $c_0 = 2.2$ cm s^{-1}, $r_0 = 4$ yr (Fig. 17).

The high skill score of this fit (correlation 0.79) shows that the essential physics are captured in Eq. (4). The parameters are similarly reasonable. For a meridional

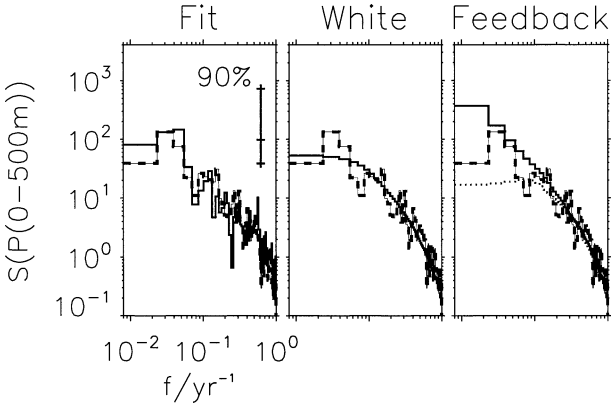

FIG. 16. Spectral power of ocean pressure at 151°E, averaged from 34° to 39°N and integrated vertically over the top 500 m of the water column. (left panel) Spectra for results of ECHO-2 (solid line) and from the best-fit solution to Eq. (4) for the wind stress curl of ECHO-2 (dashes connected by thin line). This spectra is repeated as a reference on the center and right panels. (center panel) The solid line shows the expected spectrum from Eq. (6) for a white frequency spectrum (while conserving the spatial coherences) of ECHO-2's Ekman pumping without air–sea feedback. (right panel) The solid line displays the solution with positive feedback estimated from results of ECHO-2. The dotted line shows results for the same feedback magnitude, but with reversed sign.

scale of 1000 km, typical of the decadal pressure signal in the ocean (Fig. 6), the value of r_0 corresponds to a horizontal eddy coefficient of 8×10^3 m^2 s^{-1}, strong, but consistent with the coarse-resolution, viscous ocean of the coupled model. The propagation speed is consistent with a first baroclinic mode in a realistic background state (Killworth et al. 1997), and within the observed range (Chelton and Schlax 1996; Miller et al. 1997). The combination of dissipation and propagation yields a decay scale $r_0 c_0$ of 2800 km and discriminates against the stronger forcing east of the date line compared to weaker forcing to the west. Dissipation also limits the delay due to Rossby waves generated in the central Pacific to 4–8 yr (1–2 times of 2800 km/2.2 cm s^{-1}), consistent with the 5-yr lag between wind stress and changes in the KOE region.

b. Stochastic forcing

The frequency spectrum of pressure in the KOE region from the coupled simulation is fit well by the spectrum predicted by Eq. (4) using wind-stress forcing from ECHO-2 (Fig. 16, left panel). Both show for periods shorter than a decade a decrease in spectral energies proportional to frequency to the power of "−2," and enhanced variability at periods of 20–30 yr. The effect of the pressure at the eastern boundary is small and is removed from the subsequent analysis.

The equivalent barotropic model (4) was then forced by an exact spectrum expected from stochastic Ekman pumping estimated as follows. The wind-stress curl F was expanded in its EOFs, then all principal components were set to a white-noise process with variances equal to the corresponding mode in the coupled model. The spatial loading patterns, capturing the spatial coherences, were retained.

The result in the KOE region reproduces the overall spectral shape and powers of the coupled model and simple model hindcast, including the fall off at high frequencies and leveling at low frequencies (Fig. 16, center panel). Thus we conclude that the overall ocean streamfunction variability in the KOE region is a response to stochastic forcing of the ocean by the atmo-

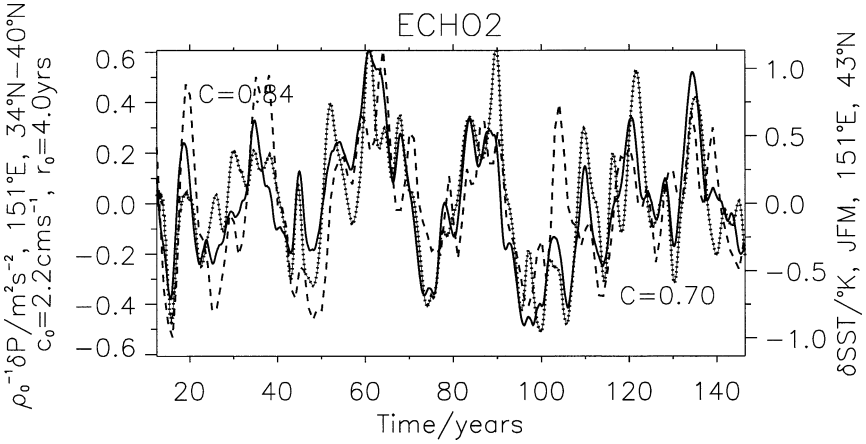

FIG. 17. Oceanic pressure (m^2 s^{-2}), averaged from the surface to a depth of 500 m and from 34° to 40°N at 151°E, just outside of the western boundary region. The solid black line is the result of ECHO-2, the connected-dot line is the best fit obtained from the equivalent barotropic model (4) forced by wind stress curl from ECHO-2 for a westward Rossby wave speed of 2.2 cm s^{-1} and a decay time of 4 yr. The correlation of the pressure from ECHO-2 and from the equivalent barotropic model is 0.84. JFM anomalies of SST (K) in the KOE region are shown as a dashed line, with ordinate on the right. The correlation of anomalies of oceanic pressure and SST is 0.7.

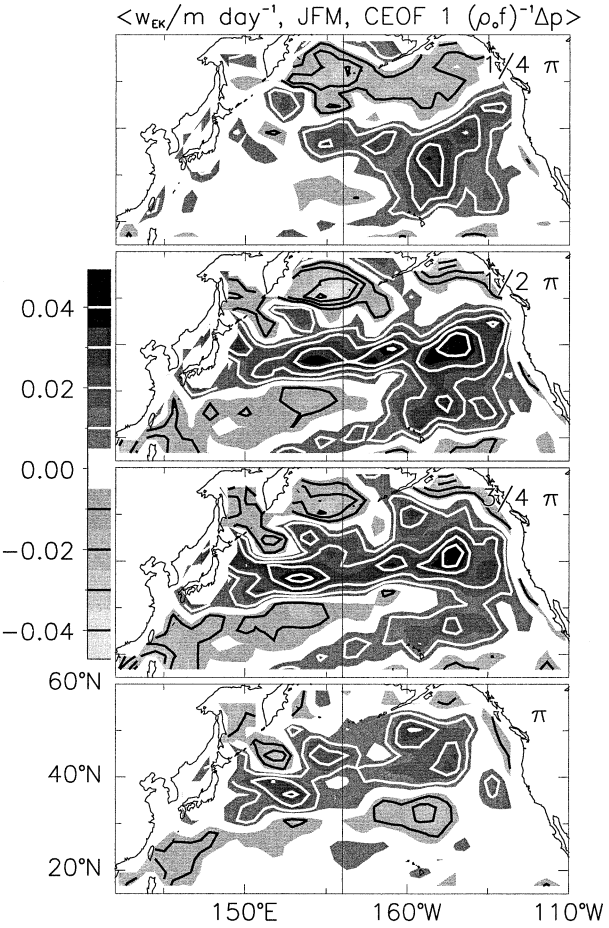

FIG. 18. Same as Fig. 6, but for winter (JFM) Ekman pumping (m day^{-1}).

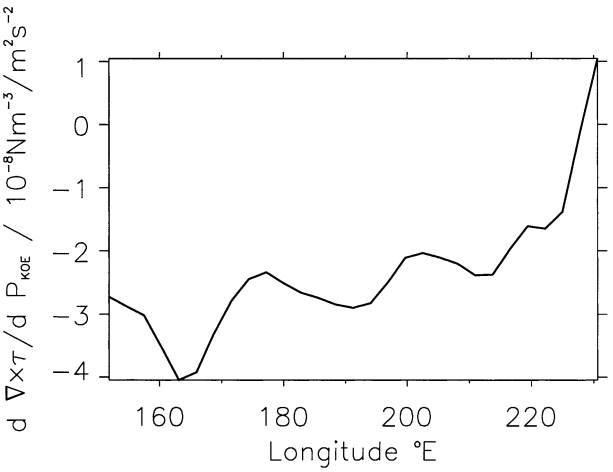

FIG. 19. Regression of annually averaged anomalies of the curl of the wind stress averaged from 34° to 41°N with anomalies of pressure in the KOE region. Abscissa depicts east longitude, units of ordinate are 10^{-8} N m^{-5} s^2.

sphere (Frankignoul et al. 1997). The stochastically forced solution, however, does not reproduce the enhanced spectral levels at 20–30-yr periods; this is consistent with results for SST using the full-physics ocean model (Pierce et al. 2001), and so we conclude that spatial resonance (Saravanan and McWilliams 1998; Neelin and Weng 1999) cannot explain the enhanced variance. Therefore Ekman pumping must have enhanced power in this spectral band due to sampling, processes external to the midlatitudes or air–sea feedbacks. The consistency of the latter process with the spectrum of KOE pressure will be determined by incorporating an ocean to atmosphere feedback in Eq. (4) and comparing the expected spectra with those of ECHO-2.

c. Ocean–atmosphere feedback

For a coupled, midlatitude ocean–atmosphere oscillation to exist, two features are required. The oceanic dynamics must introduce a delay to set the decadal timescale, and oceanic and/or atmospheric dynamics must reverse the phase of the oscillation after the delay. Latif and Barnett (1994, 1996) proposed the following mechanism to explain a 20-yr period of the midlatitude North Pacific. A single pattern of SST anomalies in the North Pacific is generated and maintained by positive feedback with the surface heat flux. The associated anomalies of the wind-stress curl lead, after a half-period (10 yr) delay due to Rossby wave propagation, to changes of the western boundary currents that reverse the initial SST anomaly and thereby the phase of the oscillation.

In ECHO-2 we find the following sequence of events. The primary SST pattern in the central North Pacific is directly forced by the atmosphere and is not affected by the adjustment of the geostrophic, ocean gyres. Hence it can neither furnish a delay nor be responsible for a negative feedback. The SST pattern in the KOE region is a delayed response to the central Pacific forcing, but is of the same sign as the central Pacific SST anomalies. By itself, this does not constitute a negative feedback. For a delayed negative feedback to exist, the atmospheric response to the oceanically induced anomalies in the KOE region has to force an atmospheric response in the North Pacific and induce ocean streamfunction anomalies of opposite polarity there.

The precipitation pattern (Fig. 15) in the western Pacific off Japan when the KOE SST signal peaks (at $\varphi_1 = 3/4\pi$ to π) suggests that the midlatitude atmosphere responds to oceanically induced anomalies in the KOE region. The associated pattern of atmospheric pressure and wind-stress curl (Fig. 18) show small perturbations in the western North Pacific, that are of the same sign as the preceding, central Pacific forcing. This suggests positive, rather than negative, feedback between KOE streamfunction (or pressure P_{KOE}) and wind stress curl via anomalies of the KOE surface heat

budget and SST. Alternatively, remote forcing at 20–30-yr timescales may explain this time sequence of wind stress curl.

To test if a positive feedback is consistent with the spectrum of P_{KOE}, the wind-stress curl in Eq. (3) is written as a superposition of two parts: a stochastic part, F_{ATMOS} due to the internal atmospheric dynamics, and a part linearly dependent on P_{KOE}

$$F(x, t) = F_{\mathrm{ATMOS}}(x, t) + \gamma(x)P_{\mathrm{KOE}}(t), \tag{5}$$

where $\gamma(x)$ is the spatially dependent regression parameter. This approach, justified by the coupled model results, is similar to the negative feedback postulated in Münnich et al. (1998) in a study of North Pacific, decadal variability in a reduced gravity model.

The Fourier components $\hat{P}_{\mathrm{KOE}}(\omega)$ as a function of frequency ω are then

$$\hat{P}_{\mathrm{KOE}}(\omega) = -\frac{f}{\beta H\rho_0}\left\{1 + \frac{f}{\beta H\rho_0}\int_{x_E}^{x_{\mathrm{KOE}}} dx'\gamma(x')\exp\left[-\left(\iota\omega + \frac{1}{r_0}\right)\frac{x' - x_{\mathrm{KOE}}}{c_0}\right]\right\}^{-1} \sum_j B_j(\omega)\int_{x_E}^{x_{\mathrm{KOE}}} dx'\Theta_j(x') \times \exp\left[-\left(\iota\omega + \frac{1}{r_0}\right)\frac{x' - x_{\mathrm{KOE}}}{c_0}\right], \tag{6}$$

where $F_{\mathrm{ATMOS}}(x, t)$ is represented by the Fourier expansion in time of its EOFs with coefficients $B_j(\omega)$ and spatial loading pattern $\Theta_j(x)$.

To estimate the spectrum expected from stochastic forcing and the feedback, both $\gamma(x)$ and $F_{\mathrm{ATMOS}}(x, t)$ were estimated from results of ECHO-2. The sign of the regression of P_{KOE} and F (Fig. 19) indicates the positive feedback is largest in the western North Pacific and decreases toward the east. The wind stress curl due to internal atmospheric processes $F_{\mathrm{ATMOS}}(x, t)$ was obtained after removal of the part accounted for by the regression with P_{KOE}.

The feedback reddens the spectrum of P_{KOE} (Fig. 16) by increasing its variance at low frequencies and moving to lower frequency the break from red to white spectral slopes. As expected, no preferred timescale is selected. At the lowest resolved frequency, the feedback leads to an overestimate of the variance. However, this spectral level of ECHO-2 is very uncertain, as it is sensitive to the method of trend removal in the results. Spectral levels predicted by Eq. (6) at 20–30-yr periods coincide with those of ECHO-2 and of its hindcast with the equivalent baroclinic model. We also tested Eq. (6) using a negative feedback, à la Latif and Barnett (1994, 1996) and Münnich et al. (1998), by reversing the sign of $\gamma(x)$. The spectrum indeed yielded a weak peak (Fig. 16, right panel), but at a period of 10 yr and with spectral levels that were reduced by one order of magnitude below the spectra of P_{KOE} of ECHO-2. The results of ECHO-2 are therefore inconsistent with a midlatitude gyre ocean–atmosphere delayed negative feedback loop. They are consistent with a positive feedback between changes of the geostrophic flow and stratification in the KOE region and the wind stress curl.

d. Global atmospheric context

The origin of the oceanic forcing at low frequencies was so far only obscurely attributed to ''internal atmospheric variability.'' While an exhaustive study of this topic is beyond the scope of this paper, it is of interest to ask whether the atmospheric patterns forcing the decadal variability in the North Pacific are restricted to this area, or have significant expression in other parts of the globe. To this end, the associated pattern of global atmospheric streamfunction at the 850-mb pressure surface was constructed. The associated pattern and decadal index explain a large part of the variance of the atmospheric streamfunction in the Tropics, and to a lesser extent in the South Pacific and Atlantic (Fig. 20). The pattern reproduces aspects of the quasi-symmetric signature of observed, low-frequency Pacific variability (Zhang et al. 1997; White and Cayan 1998; Garreaud and Battisti 1999). The high correlation in the region of the South Pacific convergence zone suggests forcing from anomalies of deep convection there.

The associated pattern of 850-mb streamfunction is very similar to the leading EOF of low-pass atmospheric streamfunction (pattern correlation 0.94 for $\varphi_1 = \pi/2$).

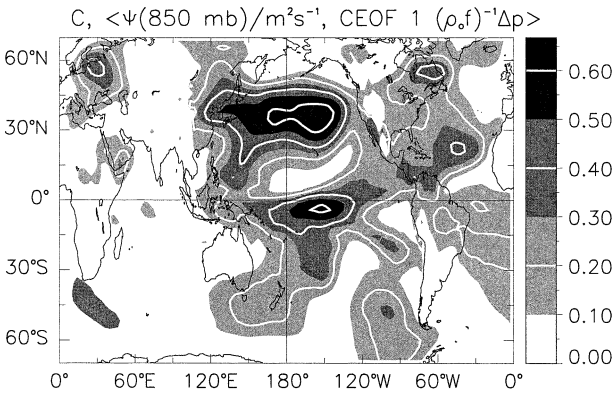

FIG. 20. Correlation of reconstruction of annually averaged atmospheric streamfunction at 850 mb from the decadal index with original data. Contour interval and shading is explained on bar on right-hand side.

The spectrum of the time series of this pattern, obtained by regression onto the unfiltered anomalies of atmospheric streamfunction, does not have any peak at a period of 20–30 yr, rather it is nearly white with a slight reddening. The forcing of oceanic decadal variability in the North Pacific is therefore either part of a near-global pattern of intrinsic atmospheric variability, which has been shown to have slightly reddish spectra (James and James 1989), or it is due to broadband ocean–atmosphere interaction in the Tropics.

e. Summary

The preponderance of variance at decadal timescales in ECHO-2 is a result of the accumulation by oceanic Rossby waves of stochastic wind-stress curl due to internal atmospheric dynamics (Frankignoul et al. 1997). The enhanced low-frequency variance in the coupled model is consistent with a positive feedback acting between KOE heat budget anomalies (driven by the oceanic streamfunction) and the wind stress over the western and central North Pacific. However, this feedback cannot explain the marginally significant spectral peak at a 20–30-yr period found in ECHO-2. This peak therefore results from samping fluctuations or processes external to the North Pacific.

8. Observations

The analysis of the decadal polarization relationship in the coupled model is in many aspects consistent with observations. These include the dominance of wintertime atmospheric forcing, the existence of two centers of action of SST anomalies (central Pacific and KOE regions), the damping effect of the latent heat flux in the KOE region, and the up to 5-yr lag between SST anomalies of like sign in the central Pacific and the KOE region due to the gyre spinup. Each of these comparisons will be discussed in the following.

a. Seasonality and sea level pressure

In the coupled model, atmospheric anomalies over the North Pacific associated with the decadal signal are largest in winter and small or insignificant in summer. Nakamura and Yamagata (1999) analyzed the associated anomaly patterns of SST and atmospheric pressure from COADS-based SST products and the National Centers for Environmental Prediction (NCEP) operational analysis from 1950 to 1992. Consistent with ECHO-2, observed anomalies of surface pressure and 500-mb geopotential height associated with SST anomalies in the central Pacific and along the subarctic frontal zones are largest in the winter season (December–February), and have no significant expression in the North Pacific during summer (June–August).

The winter sea level pressure (SLP) pattern of ECHO-2 (Fig. 8) and observations (Nakamura et al. 1997; Trenberth 1990) show both largest centers of action east of the date line around 40°N. The observed magnitude of SLP changes of approximately 3 mb between the epochs 1972–76 and 1972–82 (Nakamura et al. 1997) and 4 mb between epochs 1977–82 and 1924–76 (Trenberth 1990) is consistent with the coupled model surface pressure perturbations of typical 2.5 mb, and maximum values of twice this number.

b. Ocean temperature anomaly patterns

In the coupled model, decadal North Pacific variability is associated with two anomaly patterns of SST, in the central North Pacific and in the KOE. Nakamura et al. (1997) analyzed COADS observation and found that the variability of SST on a timescale of 7 yr and longer has centers of action along the subtropical and subpolar fronts (see also Deser and Blackmon 1995). These locations correspond very well with the simulated patterns. In the simulation, however, the KOE pattern is confined to the west of the date line, while the subarctic frontal pattern of Nakamura et al. (1997) extends across the date line. This discrepancy in the zonal extent of the KOE anomalies, noted by Pierce et al. (2001) and possibly caused by high model friction, suggests that the coupled model may underestimate the role of ocean–atmosphere feedback.

The patterns of streamfunction anomalies in the model are consistent with observed dynamic height changes before and after 1980 (Deser et al. 1999). A weak observed anomaly centered at 30°N, and a second, stronger one at 40°N have their counterparts in the coupled model, as evidenced by differencing the states at $\varphi_1 = \pi/2$ to $3\pi/4$ of Fig. 6.

While not emphasized here, decadal anomalies of SST in the central North Pacific are subducted in the coupled model (Schneider et al. 1999b; Pierce et al. 2001) in accordance with observations of ocean temperature (Deser et al. 1996; Schneider et al. 1999a) and heat content (Tourre et al. 1999).

c. Latent heat flux

In the coupled model, the net surface heat flux in the KOE region damps the oceanically induced anomalies of SST, primarily by the latent flux. North Pacific hindcasts forced by observed wind stress (Xie et al. 2000) and by observed wind stress and surface heat fluxes (Miller et al. 1998) show that KOE SST anomalies result from changes of the ocean induced by preceding wind stress over the North Pacific, consistent with the results of the coupled model. In the western North Atlantic, Battisti et al. (1995) found similarly that the surface heat flux damps anomalies of SST implicating oceanic processes for their generation.

Cayan (1992) estimated the latent heat flux over the North Pacific from COADS observations. In the KOE region, winter anomalies of observed latent heat flux

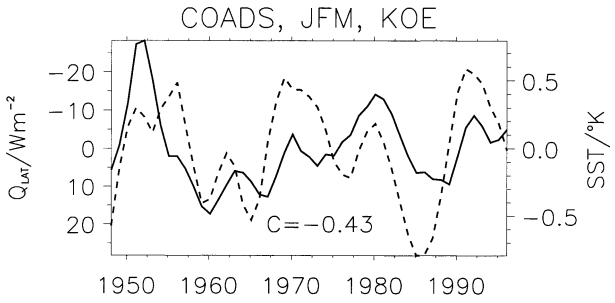

FIG. 21. Yearly time series of KOE JFM anomalies of observed latent heat flux (W m^{-2}, left ordinate, note inverted axis) and SST (K, dashed line, right ordinate). Correlation of the variables is −0.43. The KOE region covers 145° to 170°E, along 40°N.

and SST (Fig. 21) are negatively correlated (−0.43) and indicate a damping of SST anomalies by −11 W m^{-2} K^{-1}. In the coupled model, the coupling of anomalies of January–February–March (JFM) SST and latent heat flux in the KOE region is consistent with observations, but tighter (correlation coefficient −0.8) and more vigorous with regression coefficient of −18 W m^{-2} K^{-1}. Thus, model and observations suggest that the ocean forces the atmosphere in this region.

d. Lag between the central Pacific and KOE

In the coupled model, anomalies of SST and streamfunction originate in the central North Pacific and precede anomalies in the KOE region by up to 5 yr (Fig. 22). Deser et al. (1999) found that anomalies of observed oceanic heat content in the western North Pacific lagged changes of wind stress associated with the 1976/77 shift by 5 yr. Similarity, Miller et al. (1998; see also Lysne and Deser 2002) concluded, based on a comparison of an ocean hindcast, atmospheric forcing, and observations of ocean temperature, that thermocline anomalies are in a quasi-Sverdrupian balance with the wind stress curl and that KOE SST lagged the 1976/77 shift by several years due to the slow adjustment of the wind-driven circulation.

Miller and Schneider (2000) found a good correlation between winter anomalies of SST in the central Pacific leading those in the KOE by 5 yr (see Figs. 22, 23). At this lag, anomalies are of like polarity. These results appear to contradict Nakamura et al. (1997) who found that the 1976/77 cooling in the central North Pacific was predated by 2 yr by cooling at the subarctic front. Inspection of their figures, however, indicates the time series of anomalies at the subtropical and subarctic fronts are also correlated with anomalies at the subtropical front leading those at the subarctic by 5–7 yr, consistent with results presented here. Thus, available observations appear consistent with the coupled model and indicate that the KOE SST anomalies result from preceding changes of the North Pacific wind stress.

To test this hypothesis further, the observed low-passed winter KOE SST anomaly time series was reconstructed from the observed wind stress using the potential vorticity equation (4). The unknown parameters of the Rossby wave phase speed c_0, decay timescale r_0 were adjusted to optimize the correlation between the observed KOE SST anomaly and results of Eq. (4) when driven by wind stress from da Silva et al. (1994), averaged from 35° to 45°N, with the climatological seasonal cycle and trend removed. The eastern boundary at the coast of California (125°W) had zero perturbations of pressure. In contrast to the model results, the best fit (Fig. 24) is obtained with very low friction, r_0 = 40 yr pointing again to the overestimation of friction in the ocean model. Consistent with the coupled model, however, the best-fit correlation was 0.75 for a westward Rossby wave phase speed of 2.3 cm s^{-1}. This result suggests that observed low-passed winter KOE SST variability is largely generated by perturbations of the win-

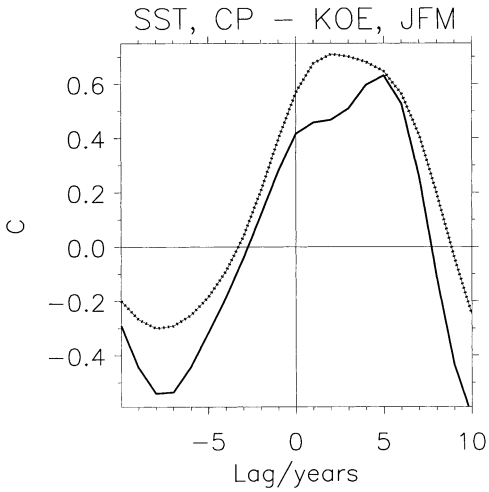

FIG. 22. Correlation between winter (JFM) time series in the central Pacific and KOE regions as a function of lag in years for observations (solid) and results from ECHO-2 (dotted connected by thin line). The ECHO-2 results were averaged over the regions CP and KOE shown in Fig. 9. Observations are based on COADS (Cayan 1992). Winter values were detrended and smoothed with a normalized 1–2–3–2–1 filter prior to calculation of the correlation. The central Pacific region is taken as an irregular shape between 30°N–45°N and 180°–150°W based on the leading North Pacific EOF. The KOE region covers 145°–170°E, along 40°N. Positive lags indicate that central Pacific time series leads.

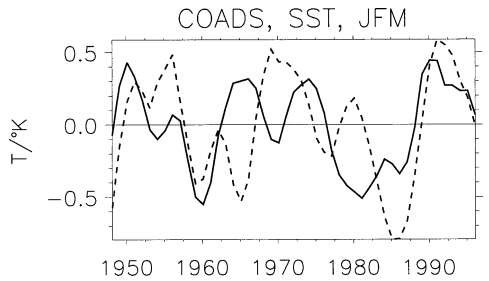

FIG. 23. Time series (top) of observed JFM anomalies of SST in the central Pacific (solid) and in the KOE (dashed).

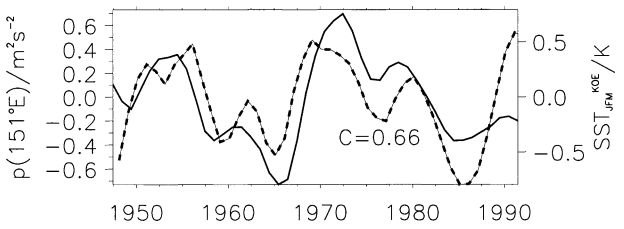

FIG. 24. Time series of KOE winter SST (JFM; dotted line, right ordinate) and pressure in the KOE region predicted from Eq. (4) forced by observed wind-stress curl (da Silva et al. 1994). Westward Rossby wave propagation speed of 2.3 cm s^{-1} was determined by maximizing the correlation between these time series (correlation 0.66), friction was not important (frictional timescale is larger than 40 yr).

tertime mixed-layer heat budget by undulations of the thermocline that were generated in previous years farther east in the North Pacific.

9. Conclusions

In the ECHO-2 coupled ocean–atmosphere model, decadal variability in the North Pacific evolves in accordance with the schematic of Miller and Schneider (2000). Changes of wintertime atmospheric pressure in the North Pacific, primarily due to intrinsic, low-frequency, and global atmospheric variability, alter the surface heat budget in the central North Pacific by changing Ekman advection and vertical mixing. This causes the development of the ''canonical'' anomaly pattern of SST where anomalies in the central North Pacific and to the north, east, and south are of opposite polarity. The central Pacific SST anomalies are subducted southwestward toward the equator.

Anomalies of Ekman pumping associated with changes of the North Pacific sea level pressure excite anomalies of the oceanic streamfunction that are a superposition of a forced response and a westward propagating component due to long Rossby waves. On average, the KOE region is affected up to 5 yr after central Pacific anomalies reach their maximum. In the KOE region, the changes of the geostrophic circulation persist yearround. During summer, subsurface KOE temperature anomalies are insulated from the atmosphere by the seasonal thermocline and attain largest values, while the SST anomalies are small. During winter, deep mixed layers bring the subsurface anomalies to the surface and lead to KOE SST anomalies of the same sign as the preceding SST anomalies in the central Pacific. The associated anomalous heating of the surface layer is vented to the atmosphere by changes of the turbulent heat fluxes, primarily the latent component. These anomalous surface conditions lead to anomalous precipitation over the western North Pacific Ocean, such that warm SSTs and increased transfer of sensible and latent heat from the ocean to the atmosphere coincide with increased precipitation. Thus the atmosphere responds locally to oceanically induced KOE surface flux anomalies.

The response of the wind stress is suggestive of a positive feedback, such that anomalies of wind-stress curl over the western North Pacific reinforce existing KOE anomalies. This conclusion is based on experiments with an equivalent barotropic ocean model that captures the dynamics of linear, forced, midlatitude Rossby waves and is successful in reproducting the results of the coupled model. Experiments with this simple model suggest that the decadal timescale of the KOE variability results from the integration along Rossby wave trajectories of stochastic forcing due to internal atmospheric dynamics. The positive feedback between oceanic pressure in the KOE region and North Pacific wind stress curl enhances the low-frequency variability of the ocean streamfunction due to a reddening of the spectrum of wind-stress curl. It does not, however, select a timescale. The lack of a negative feedback and the absence of a closed feedback loop are inconsistent with the assumptions often invoked in simple coupled models of North Pacific decadal variability. Instead, they are consistent with the stochastically forced ocean model of Frankignoul et al. (1997) combined with a local atmospheric response to SST that acts as a positive feedback.

Comparisons with observations confirm the coupled model results. In both observations and model, decadal anomalies of atmospheric forcing and SST are largest during winter. The SST anomalies occur in two centers of action: first in the central North Pacific, and then, with like sign and a lag of up to 5 yr, in the KOE region. There, the latent heat flux damps the SST anomalies consistent with an oceanic, rather than an atmospheric, generation mechanism. This points to the adjustment of the wind-driven, geostrophic circulation as link between anomalies in the central Pacific and in the KOE region with a 5-yr lag. Seager et al. (2001) concluded similarily that observed KOE SST anomalies in an North Pacific hindcast result from the adjustment of the wind-driven ocean circulation. This implies that observed anomalies in the KOE region can be predicted from the preceding wind stress forcing over the central North Pacific (Schneider and Miller 2001).

The results of the coupled model, while consistent with available observations, have to be viewed in light of the shortcomings of this integration. The 128-yr run includes only a few realizations of decadal variations (as in observations) and the ocean model has a coarse resolution and high diffusion. While the model results suggest a robust, local feedback in the KOE region between SST, turbulent air–sea heat fluxes and precipitation that is found also in atmospheric general circulation models forced with prescribed SST anomalies (Rodwell et al. 1999; Watanabe and Kimoto 2000b), the nature and importance of the associated response of the wind-stress curl is less certain. A longer run might reveal that the enhanced variability at a period of 20–30 yr in this run was due to sampling or due to processes external to the midlatitude ocean. The existence of a

positive feedback between KOE oceanic streamfunction and Ekman pumping could be easily tested in a longer integration since the enhanced variance and reddening of atmospheric spectra should persist at lower frequencies.

The coarse resolution and high mixing of the ocean model only crudely represent western boundary processes, and might limit the effect of the adjustment of the wind-driven circulation to the immediate area east of Japan. With better resolution and less mixing, this effect might extend farther to the east and, due to its larger area, be more efficient in forcing a large-scale response of the atmosphere.

The results of this study give some guidance for further investigations of the atmospheric response to midlatitude anomalies of SST and the mixed layer heat budget. Typically, this response is investigated by prescribing SST anomaly patterns in an atmospheric general circulation model. However, in the central North Pacific, the anomalous SST patterns are forced by the anomalous winds, rather than force the anomalous atmospheric state. Even in the KOE region, the anomalous perturbations of SST result from a balance of oceanically induced changes of mixing and turbulent air–sea fluxes. Prescribing SST in a general circulation model is therefore not a consistent approach to determining local and remote atmospheric response (Barsugli and Battisti 1998; Bretherton and Battisti 2000). Rather, the forcing of the ocean's surface heat budget by the adjustment of the oceanic streamfunction should be simulated by, at minimum, a coupled atmospheric general circulation and slab ocean model. In this case, SST and the atmosphere could find a combined response to the oceanically induced forcing. Such an experiment was performed by Yulaeva et al. (2001) with the National Center for Atmospheric Research (NCAR) GCM coupled to a slab ocean model. They found a significant local response consistent with the ECHO-2 coupled model (in precipitation and air–sea heat fluxes) and a remote response over the central Pacific and North America.

In addition, since Ekman advection forces anomalies of SST in the central Pacific on decadal timescales, its effect on the prescribed SST field of AGCM experiments needs to be considered in addition to the eventual response of the gyre to changes of Ekman pumping. Pierce et al. (2001) suggest that an SST anomaly pattern in the North Pacific forces a pattern of wind-stress curl that would counteract the initial SST anomaly via changes of the oceanic gyre. Comparison of the prescribed SST pattern and the zonal wind-stress response reveals that temperature advection due to the Ekman drift would damp the prescribed SST pattern. Thus, in addition to a slow feedback due to the adjustment of the geostrophic gyres, there is a fast local negative feedback due to Ekman advection that will tend to destroy this initial SST anomaly.

One additional complication to determining the atmospheric response to oceanically driven KOE SST anomalies is the strong seasonality of the atmosphere and upper-ocean mixed layer. Peng et al. (1997) showed that the atmospheric response to SST anomalies is very sensitive to the background state and therefore the season. The coupled model results presented here indicate that the coupling of the oceanic streamfunction and SST (or surface heat budget) similarly undergoes a strong seasonal modulation. The timing of a sensitive atmospheric state and the structure of the oceanic mixed layer that allows the oceanic streamfunction to influence the surface heat budget might therefore be central in determining the strength and structure of the atmospheric response. In fact, the venting of heat might be intermittent and occur mainly during times of rapid entrainment. Mean fields of SST, the surface heat budget, and the atmosphere might therefore not represent the situation during coupling. This caveat depends critically on the relative roles of upper-ocean mixing and upper-ocean advection. In ECHO-2 this balance is shifted toward the role of mixing. The extent to which this is a robust result remains to be determined.

Despite these complications, the important role of anomalies in the KOE region and the sequence of events associated with enhanced variance in the decadal band suggest that multiyear predictions are possible based in the history of the wind stress, and state of the oceanic streamfunction (Schneider and Miller 2001). Prediction of oceanic temperature anomalies in the KOE region several years in advance could greatly aid the study of sardine fisheries (Kawasaki and Omori 1995; Yasuda et al. 1999) and zooplankton populations (Sugimoto and Tadokoro 1997; Mackas and Tsuda 1999) that are sensitive to oceanic temperature. Likewise, if KOE SST anomalies drive an atmospheric result in nature that is similar to the coupled model, precipitation over the northwestern North Pacific (and perhaps concomitant climate anomalies over the Northern Hemisphere) could also be predicted at several-year lead times. Thus, even in the absence of a closed feedback loop, the time horizon of such predictions is several years and could be of value to society.

Acknowledgments. We are grateful for grants from the National Science Foundation (OCE-9711265 and OCE00-82543), the Department of Energy (DE-FG03-98ER62605), and the National Oceanic and Atmospheric Administration, Department of Commerce, under grants NA77RJ0453 and NA47GP0188. The views expressed herein are those of the authors and do not necessarily reflect the views of NOAA or any of its subagencies. The simulations were executed at NCAR's Scientific Computing Division (SCD) and Climate Simulation Laboratory (CSL), supplemented with runs at the National Energy Research Scientific Computing Center (NERSC). The coupled model was generously made available by the Max-Planck-Institut für Meteorologie, Hamburg, Germany, and Mojib Latif. We thank Bruce Cornuelle, Elena Yulaeva, Tim Barnett, and our

many colleagues for valuable discussions. We greatly appreciate the valuable comments provided in the reviews by Hisashi Nakamura and the second referee.

REFERENCES

Akimoto, K., M. Ooi, and T. Awaji, 1996: Interannual variability of the Kuroshio transport in response to the wind stress field over the North Pacific: its relations to the path variations south of Japan. *J. Geophys. Res.,* **101,** 14 057–14 071.

Alexander, M. A., and C. Deser, 1995: A mechanism for the recurrence of wintertime midlatitude SST anomalies. *J. Phys. Oceanogr.,* **25,** 122–137.

——, ——, and M. S. Timlin, 1999: The reemergence of SST anomalies in the North Pacific Ocean. *J. Climate,* **12,** 2419–2433.

Barnett, T., 1983: Interaction of the monsoon and Pacific trade wind system at interannual time scales. Part I: The equatorial zone. *Mon. Wea. Rev.,* **111,** 756–773.

——, D. W. Pierce, M. Latif, D. Dommenget, and R. Saravanan, 1999a: Interdecadal interactions between the tropics and midlatitudes in the Pacific basin. *Geophys. Res. Lett.,* **26,** 615–618.

——, ——, R. Saravanan, N. Schneider, D. Dommenget, and M. Latif, 1999b: Origins of the midlatitude Pacific decadal variability. *Geophys. Res. Lett.,* **26,** 1453–1456.

Barsugli, J. J., and D. S. Battisti, 1998: The basic effects of a atmosphere–ocean thermal coupling on midlatitude variability. *J. Atmos. Sci.,* **55,** 477–493.

Battisti, D. S., U. S. Bhatt, and M. A. Alexander, 1995: A modeling study of the interannual variability in the wintertime North Atlantic Ocean. *J. Climate,* **8,** 3067–3083.

Bretherton, C. S., and D. S. Battisti, 2000: An interpretation of the results from atmospheric general circulation models forced by the time history of the observed sea surface temperature distribution. *Geophys. Res. Lett.,* **27,** 767–770.

Cayan, D. R., 1992: Variability of latent and sensible heat fluxes estimated using bulk formulae. *Atmos.–Ocean,* **30,** 1–42.

Cessi, P., 2000: Thermal feedback on wind stress as a contributing cause of climate variability. *J. Climate,* **13,** 232–244.

Chelton, D. B., and M. B. Schlax, 1996: Global observations of oceanic Rossby waves. *Science,* **272,** 234–238.

da Silva, A. M., C. C. Young, and S. Levitus, 1994: *Algorithms and Procedures.* Vol. 1, *Atlas of Surface Marine Data 1994,* NOAA Atlas NESDIS 6, 83 pp.

Deser, C., and M. L. Blackmon, 1995: On the relationship between tropical and North Pacific sea surface temperature variations. *J. Climate,* **8,** 1677–1680.

——, M. A. Alexander, and M. S. Timlin, 1996: Upper-ocean thermal variations in the North Pacific during 1970–1991. *J. Climate,* **9,** 1840–1855.

——, ——, and ——, 1999: Evidence for a wind-driven intensification of the Kuroshio Current Extension from the 1970s to the 1980s. *J. Climate,* **12,** 1697–1706.

Ebbesmeyer, C. C., D. R. Cayan, D. R. McLain, F. H. Nichols, D. H. Peterson, and K. T. Redmond, 1991: 1976 step in the Pacific climate: Forty environmental changes between 1968–75 and 1977–84. *Proc. Seventh Annual Pacific Climate Workshop,* Pacific Grove, CA, California Dept. of Water Resources, Interagency Ecology Studies Program Rep. 26, 115–126.

Frankignoul, C., P. Müller, and E. Zorita, 1997: A simple model of the decadal response of the ocean to stochastic wind forcing. *J. Phys. Oceanogr.,* **27,** 1533–1546.

——, E. Kestenare, N. Sennechael, G. de Coetlogon, and F. D'Andrea, 2000: On decadal-scale ocean–atmosphere interactions in the extended ECHAM1/LSG climate simulation. *Climate Dyn.,* **16,** 333–354.

Frey, H., M. Latif, and T. Stockdale, 1997: The coupled model ECHO-2. Part I: The tropical Pacific. *Mon. Wea. Rev.,* **125,** 703–720.

Garreaud, R. D., and D. S. Battisti, 1999: Interannual (ENSO) and interdecadal (ENSO-like) variability in the Southern Hemisphere tropospheric circulation. *J. Climate,* **12,** 2113–2123.

Gershunov, A., and T. P. Barnett, 1998: Interdecadal modulation of ENSO teleconnections. *Bull. Amer. Meteor. Soc.,* **79,** 2715–2725.

Goodman, J., and J. Marshall, 1999: A model of decadal middle-latitude atmosphere–ocean coupled modes. *J. Climate,* **12,** 621–641.

Graham, N. E., T. P. Barnett, R. Wilde, M. Ponater, and S. Schubert, 1994: Low-frequency variability in the winter circulation over the Northern Hemisphere. *J. Climate,* **7,** 1416–1442.

Hanawa, K., S. Ishizaki, and Y. Tanimoto, 1996: Examination of the strengthening of wintertime mid-latitude westerlies over the North Pacific in the 1970s. *J. Meteor. Soc. Japan,* **74,** 715–721.

James, I. N., and P. M. James, 1989: Ultra-low-frequency variability in a simple atmospheric circulation model. *Nature,* **342,** 53–55.

Jin, F. F., 1997: A theory of interdecadal climate variability of the North Pacific ocean–atmosphere system. *J. Climate,* **10,** 1821–1835.

Kawasaki, T., and M. Omori, 1995: Possible mechanisms underlying fluctuations in the far-eastern sardine population inferred from time-series of 2 biological traits. *Fish Oceanogr.,* **4,** 238–242.

Killworth, P. D., D. B. Chelton, and R. A. de Szoeke, 1997: The speed of observed and theoretical long planetary waves. *J. Phys. Oceanogr.* **27,** 1946–1966.

Latif, M., and T. P. Barnett, 1994: Causes of decadal climate variability over the North Pacific and North America. *Science,* **266,** 634–637.

——, and ——, 1996: Decadal climate variability over the North Pacific and North America: Dynamics and predictability. *J. Climate,* **9,** 2407–2423.

Levitus, S., 1982: *Climatological Atlas of the World Ocean.* NOAA Prof. Paper 13, 173 pp.

Lysne, J., and C. Deser, 2002: Wind-driven thermocline variability in the Pacific: A model–data comparison. *J. Climate,* in press.

Mackas, D. L., and A. Tsuda, 1999: Mesozooplankton in the eastern and western subarctic Pacific: Community structure, seasonal life histories, and interannual variability. *Progress in Oceanography,* Vol. 43, Pergamon, 335–363.

Mantua, N. J., S. R. Hare, Y. Zhang, J. M. Wallace, and R. C. Francis, 1997: A Pacific interdecadal climate oscillation with impacts on salmon production. *Bull. Amer. Meteor. Soc.,* **78,** 1069–1079.

Miller, A. J., and N. Schneider, 2000: Interdecadal climate regime dynamics in the North Pacific Ocean: Theories, observations and ecosystem impacts. *Progress in Oceanography,* Vol. 27, Pergamon, 257–260.

——, D. R. Cayan, T. P. Barnett, N. E. Graham, and J. M. Oberhuber, 1994: Interdecadal variability of the Pacific Ocean: Model response to observed heat flux and wind stress anomalies. *Climate Dyn.,* **9,** 287–302.

——, W. B. White, and D. R. Cayan, 1997: North Pacific thermocline variations on ENSO timescales. *J. Phys. Oceanogr.,* **27,** 2023–2039.

——, D. R. Cayan, and W. B. White, 1998: A westward intensified decadal change in the North Pacific thermocline and gyre-scale circulation. *J. Climate,* **11,** 3112–3127.

Münnich, M., M. Latif, S. Venzke, and E. Maier-Reimer, 1998: Decadal oscillations in a simple coupled model. *J. Climate,* **11,** 3309–3319.

Nakamura, H., and T. Yamagata, 1999: Recent decadal SST variability in the northwestern Pacific and associated atmospheric anomalies. *Beyond El Niño: Decadal and Interdecadal Climate Variability,* A. Navarra, Ed., Springer Verlag, 49–72.

——, G. Lin, and T. Yamagata, 1997: Decadal climate variability in the North Pacific during recent decades. *Bull. Amer. Meteor. Soc.,* **78,** 2215–2225.

Namias, J., and R. M. Born, 1970: Temporal coherence in North Pacific sea surface temperature patterns. *J. Geophys. Res.,* **75,** 5952–5955.

——, and ——, 1974: Further studies of temporal coherence in North Pacific sea surface temperatures. *J. Geophys. Res.,* **79,** 797–798.

Neelin, J. D., and W. J. Weng, 1999: Analytical prototypes for ocean–atmosphere interaction at midlatitudes. Part I: Coupled feedbacks as a sea surface temperature dependent stochastic process. *J. Climate,* **12,** 697–721.

Nitta, T., and S. Yamada, 1989: Recent warming of tropical sea surface temperature and its relationship to the northern hemisphere circulation. *J. Meteor. Soc. Japan,* **67,** 375–383.

Peng, S., W. A. Robinson, and M. P. Hoerling, 1997: The modeled atmospheric response to midlatitude SST anomalies and its dependence on background circulation states. *J. Climate,* **10,** 971–987.

Pierce, D. W., T. Barnett, and M. Latif, 2000: Connections between the Pacific Ocean Tropics and midlatitudes on decadal timescales. *J. Climate,* **13,** 1173–1194.

——, ——, N. Schneider, R. Saravanan, D. Dommenget, and M. Latif, 2001: The role of ocean dynamics in producing decadal climate variability in the North Pacific. *Climate Dyn.,* **18,** 51–70.

Qiu, B., and R. X. Huang, 1995: Ventilation of the North Atlantic and North Pacific: Subduction versus obduction. *J. Phys. Oceanogr.,* **25,** 2374–2390.

Robertson, A. W., 1996: Interdecadal variability over the North Pacific in a multi-century climate simulation. *Climate Dyn.,* **12,** 227–241.

Rodwell, M. J., D. P. Rowell, and C. K. Folland, 1999: Oceanic forcing of the wintertime North Atlantic Oscillation and European climate. *Nature,* **398,** 320–323.

Roeckner, E., and Coauthors, 1996: The atmospheric general circulation model ECHAM-4: Model description and simulation of present-day climate. DKRZ Tech. Rep. 218, 99 pp. [Available from DKRZ, Bundesstr. 55, 20146 Hamburg, Germany.]

Saravanan, R., and J. C. McWilliams, 1998: Advective ocean–atmosphere interaction: An analytical stochastic model with implications for decadal variability. *J. Climate,* **11,** 165–188.

Schneider, N., 2000: A decadal spiciness mode in the Tropics. *Geophys. Res. Lett.,* **27,** 257–260.

——, and A. J. Miller, 2001: Predicting western North Pacific Ocean climate. *J. Climate,* **14,** 3997–4002.

——, ——, M. A. Alexander, and C. Deser, 1999a: Subduction of decadal North Pacific temperature anomalies: Observations and dynamics. *J. Phys. Oceanogr.,* **29,** 1056–1070.

——, S. Venzke, A. J. Miller, D. W. Pierce, T. Barnett, C. Deser, and M. Latif, 1999b: Pacific thermocline bridge revisited. *Geophys. Res. Lett.,* **26,** 1329–1332.

Seager, R., Y. Kushnir, N. Naik, M. A. Cane, and J. A. Miller, 2001: Wind-driven shifts in the latitude of the Kuroshio–Oyashio Extension and generation of SST anomalies on decadal timescales. *J. Climate,* **14,** 4249–4265.

Sturges, W., and B. G. Hong, 1995: Wind forcing of the Atlantic thermocline along 32°N at low frequencies. *J. Phys. Oceanogr.,* **25,** 1706–1715.

Sugimoto, T., and K. Tadokoro, 1997: Interannual-interdecadal variations in zooplankton biomass, chlorophyll concentration and physical environment in the subarctic Pacific and Bering Sea. *Fish. Oceanogr.,* **6,** 74–93.

Talley, L. D., 1999: Simple coupled midlatitude climate models. *J. Phys. Oceanogr.,* **29,** 2016–2037.

Tanimoto, Y., N. Iwasaka, K. Hanawa, and Y. Toba, 1993: Characteristic variations of sea surface temperature with multiple timescales in the North Pacific. *J. Climate,* **6,** 1153–1160.

Tourre, Y., W. B. White, and Y. Kushnir, 1999: Evolution of interdecadal variability in sea level pressure, sea surface temperature, and upper-ocean temperature over the Pacific Ocean. *J. Phys. Oceanogr.,* **29,** 1528–1541.

Trenberth, K. E., 1990: Recent observed interdecadal climate changes in the Northern Hemisphere. *Bull. Amer. Meteor. Soc.,* **71,** 988–993.

——, and J. W. Hurrel, 1994: Decadal atmosphere–ocean variations in the Pacific. *Climate Dyn.,* **9,** 303–319.

Venzke, S., M. Münnich, and M. Latif, 2000: On the predictability of decadal changes in the North Pacific. *Climate Dyn.,* **16,** 379–392.

Vimont, D. J., D. S. Battisti, and A. C. Hirst, 2001: Footprinting: A seasonal connection between the Tropics and mid-latitudes. *Geophys. Res. Lett.,* **28,** 3923–3926.

Watanabe, M., and M. Kimoto, 2000a: Behavior of midlatitude decadal oscillations in a simple atmosphere–ocean system. *J. Meteor. Soc. Japan,* **78,** 441–460.

——, and ——, 2000b: Atmosphere–ocean thermal coupling in the North Atlantic: A positive feedback. *Quart. J. Roy. Meteor. Soc.,* **126,** 3343–3369.

White, W. B., and D. R. Cay, 1998: Quasi-periodicity and global symmetries in interdecadal upper ocean temperature variability. *J. Geophys. Res.,* **103,** 21 335–21 354.

Xie, S. P., T. Kunitani, A. Kubokawa, M. Nonaka, and S. Hosoda, 2000: Interdecadal thermocline variability in the North Pacific for 1958–97: A GCM simulation. *J. Phys. Oceanogr.,* **30,** 2798–2813.

Yasuda, I., H. Sugisaki, Y. Watanabe, S. S. Minobe, and Y. Oozeki, 1999: Interdecadal variations in Japanese sardine and ocean/climate. *Fish. Oceanogr.,* **8,** 18–24.

Yulaeva, E., N. Schneider, D. W. Pierce, and T. Barnett, 2001: Modeling of North Pacific climate variability forced by oceanic heat fluxes anomalies. *J. Climate,* **14,** 4027–4046.

Zhang, Y., J. M. Wallace, and D. S. Battisti, 1997: ENSO-like interdecadal variability: 1900–93. *J. Climate,* **10,** 1004–1020.